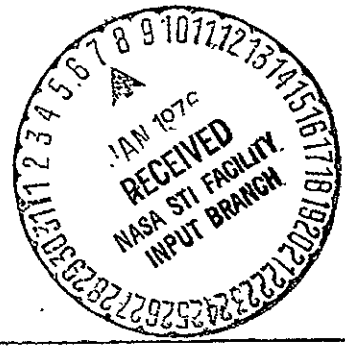

CORNELL UNIVERSITY

Center for Radiophysics and Space Research

ITHACA, N. Y.

CRSR 613

FAR INFRARED SPECTROSCOPY OF H II REGIONS

Dennis Brien Ward

November 1975

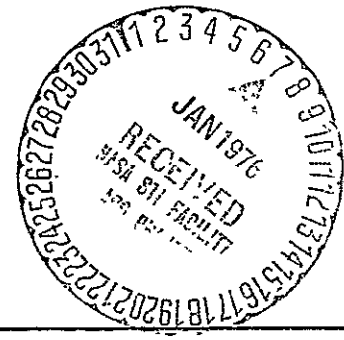

FAR INFRARED SPECTROSCOPY OF H II REGIONS

A Thesis

Presented to the Faculty of the Graduate School

of Cornell University for the Degree of

Doctor of Philosophy

by

Dennis Brien Ward

January 1976

FAR INFRARED SPECTROSCOPY OF H II REGIONS

Dennis Brien Ward, Ph.D.
Cornell University, 1976

A fully liquid helium cooled grating spectrometer has been developed for far infrared observations from the NASA Lear Jet. This instrument has been used in observations of the galactic H II regions M42 and M17.

In this thesis the instrument is described, and the results of various performance tests and calibrations are presented. The methods employed in observations from the Lear Jet are described, and the data analysis procedures are discussed.

The results of a search for the (O III) 88.16 micron fine structure line are presented. The intensity of the line in M17 is reported, and an upper limit given for the intensity in M42. These results are compared with theoretical predictions, and future applications of infrared line observations are discussed.

Coarse resolution spectra of M42 and M17 from 45 to 115 microns are also presented. The emission from M42 is shown to be a very smooth function of wavelength, closely fitting the wavelength dependence of a 105°K graybody. The spectrum of M17 is very different, having a bump at ∿75 microns and a general far infrared excess. The observed spectrum is compared to the predictions of models for M17.

BIOGRAPHICAL SKETCH

Dennis Brien Ward was born on [redacted] in [redacted], [redacted]. In May, 1969 he received a B.Sc. with First Class Honours in Physics from the University of Alberta, and he entered graduate school at Cornell University the following September. During his graduate work he was supported by a research assistantship, and for three years by a National Research Council of Canada Fellowship. He has authored or co-authored several papers describing results obtained in infrared observations from the NASA Lear Jet.

ACKNOWLEDGEMENTS

My greatest debt of gratitude is to Professor Martin Harwit and Professor James Houck. Martin headed this project, and his advice and encouragement kept me going during the rather depressing and data-less early days of the Lear Jet observing program. Jim was always available to give advice concerning the instrument, which he originally designed, and was responsible for the development of much of the equipment used during observations.

Many others have done much to make the observations a success. Particularly I owe much to those who flew with me in the aircraft--Dan Briotta, Brian Dennison, George Gull, Mike Jacobson and the late Leon King. Brian also assisted in data reduction, and George built some of the electronics Dr. Carl Frederick did much of the early modification of the instrument.

Dave Schaack, Gerry Stasavage and Geoff Bodwin were always willing and usually able to answer my many questions of a technical nature, and the work of Dr. W.J. Moore helped to improve the detectors and preamplifiers.

Barbara Boettcher (figures), Herman Eckelmann (photographs) and Mrs. C. Sheehan (typing) did a rapid and accurate job of preparing the final copy of the thesis. To them my thanks.

My thanks also to Dr. Y. Terzian and Dr. K. Greisen, who served on my special committee.

Finally, I would like to express my appreciation to the staff at NASA Ames who made the observations possible, particularly Robert H. Mason, Glenn Stinnett, Dr. E. Erickson and Robert Cullum.

This work was supported by NASA contract NGR 33-010-146.

TABLE OF CONTENTS

CHAPTER		Page
I	INTRODUCTION.	1
II	THE SPECTROMETER.	4
	History and Success of the Instrument	4
	Description of the Spectrometer	6
	General Construction and Cryogenics	6
	Grating Drive and Gratings.	10
	Filters and Detectors	13
	Preamplifiers	15
	Instrument Configuration--Earlier Flight Series	16
	Instrumental Tests and Calibrations	18
	Wavelength Calibration.	18
	Resolution.	20
	Beam Shape Determination.	26
	Linearity	28
	Scattered Light	34
	Sensitivity as a Function of Wavelength . .	37
	Filter Tests.	40
III	OBSERVING PROCEDURE AND DATA ANALYSIS	
	Field Trips	41
	The Lear Jet Telescope.	41
	Observing Procedure	45
	Data Acquisition System	45
	Preflight Testing	46
	Initial Flight Testing.	46
	Procedure During Data Flights	49
	Data Analysis	52
	Averaging and Normalization	53
	Lunar Calibrations.	54
	Error Analysis.	57
IV	HIGH RESOLUTION OBSERVATIONS OF H II REGIONS.	59
	Infrared Fine Structure Lines	59
	Observations of M42	62
	Observations of M17	65
	Comparison to Theoretical Predictions	68

CHAPTER Page

Applications of Infrared Fine Structure Measurements 71
The (O III) 88.16μ Line 71
Future Applications of Infrared Lines 77

V COARSE RESOLUTION OBSERVATIONS OF H II REGIONS 80

M42 Observations 80
The March 1974 Field Trip 80
The November 1974 Field Trip 82
The March-April 1975 Field Trip 82
M17 Observations--The March-April 1975 Field Trip 84
Discussion of the M42 and M17 Spectra 87
Calibrations 87
Dust Models 91
M42 91
M17 93
Future Observations 98

BIBLIOGRAPHY 100

LIST OF TABLES

TABLE		Page
2-1	Spectrometer Parameters	11
2-2	Grating Parameters	12
3-1	Field Trips	42
4-1	Predicted and Observed Intensities for (O III) 88.16μ	72
4-2	Predicted Line Strengths for the Orion Nebula--Simpson (1975)	78
5-1	Some Observable H II Regions	99

LIST OF FIGURES

FIGURE		Page
2-1	Spectrometer Light Path.	7
2-2	View of the Inside of the Spectrometer	8
2-3	The Spectrometer Mounted on the Dewar.	9
2-4	Detector Blocks, Preamplifiers and Filter Mounts	14
2-5	Preamplifier Schematic	17
2-6	Calculated Atmospheric Transmission.	19
2-7	Resolution Tests.	21
2-8	Resolution Changes with Entrance Slit Size . .	23
2-9	Zero Order Scans.	24
2-10	Beam Profile	27
2-11	Basic Detector and Preamplifier Circuit. . . .	29
2-12	Short Wavelength Detector--Nonlinearity. . . .	32
2-13	Long Wavelength Detector--Nonlinearity.	33
2-14	Lunar Spectrum--1.45μ Resolution	36
2-15	Sensitivity as a Function of Wavelength. . . .	38
3-1	The Lear Telescope	44
3-2	The Electronics Rack	47
3-3	Flight Electronics	48
3-4	Typical Lunar Calibration Spectrum	56
4-1	Lower Energy Levels for Electron Configuration p^1 to p^5	60
4-2	Spectrum of Orion Nebula at 1.3μ Resolution Around the (O III) 88.16μ Line	63
4-3	Spectra of M17, M42, Venus and the Moon at 1.3μ Resolution Around the (O III) 88.16μ Line.	66
4-4	Emissivity of O III and N II Fine Structure Lines.	74
5-1	Spectrum of M42 From March 1974 Field Trip . .	81
5-2	Spectrum of M42 From November 1974 Field Trip.	83
5-3	Spectra of M17 and M42 From the March-April 1975 Field Trip.	85
5-4	Spectrum of Venus From the March-April 1975 Field Trip.	90

CHAPTER I

INTRODUCTION

Broadband observations carried out from aircraft, balloons and sounding rockets have discovered a large number of sources which emit strongly in the far infrared (Harper and Low, 1971; Hoffman et al., 1971; Emerson et al., 1973; Soifer et al., 1972). These sources are primarily associated with galactic H II regions. The source of the emission is generally believed to be thermal emission from interstellar dust, but the composition, distribution and temperature of this material are not well known.

Broadband observations of brightness temperature cannot determine the actual temperature of the dust, since the objects are either optically thin in the far infrared, or contain dense clumps buried in an optically thin medium. Therefore, temperatures must be derived from the observed spectrum. Such temperatures have been determined by Harper (1974) for a number of H II regions using broadband fluxes at various effective wavelengths, but this approach is very inaccurate. In addition to the errors in the measurements, which are of order 25% including the calibration errors, the effective wavelength of the filters depends on the source spectrum. Hence some sort of spectrum has to be chosen, and for simplicity it is usually a blackbody function. This ignores the

fact that the emission must come at least in part from an optically thin region, where emissivity effects of the form λ^{-n} will probably play a role. As well, the source may have several components of different temperature and optical depth.

To get accurate temperatures, narrower band spectral data is necessary. If the source emission does indeed follow a blackbody function wavelength dependence, the temperature can be accurately determined from the peak of the spectrum. However, if the spectrum is more complicated, considerably more information will be obtained. The emissivity is expected to fall at long wavelengths for most grain materials, but this effect occurs above a critical wavelength which is different for different materials. Hence if emissivity effects occur, information regarding the composition of the grains can be inferred. If bumps of dips appear in the spectrum, they are bound to yield some information concerning temperature, composition or distribution of the matter.

A further possibility is that far infrared spectra may show line emission from atoms or molecules. Far infrared fine structure lines from ions have been predicted to be strong in H II regions by Petrosian (1970) and Simpson (1975), and would be useful in determining the electron density and ionic abundances in these regions.

In the chapters to follow, a program of observations to determine the far infrared spectra of H II regions is described.

In Chapter II a description is given of the construction of a liquid helium cooled grating spectrometer designed to make observations from the NASA Lear Jet. The results of tests of the instrument are presented, and some problems described.

In Chapter III, the observing procedure on the Lear Jet telescope is described. The method of data analysis is also discussed.

Chapter IV presents the results from a search for the (O III) 88.16μ line in M17 and M42. An upper limit on the emission in this line from M42 is obtained, and the line detection in M17 is described. This is the first detection of a far infrared line in an H II region. The results are compared to theoretical predictions, and future applications of fine structure line observations are discussed.

Chapter V contains the coarse resolution results from M17 and M42. Calibration problems associated with the spring 1975 observations are discussed. The spectra obtained are compared to models for dust emission.

CHAPTER II

THE SPECTROMETER

The first section of this chapter will give a short history of the development of the instrument. In the second section, the spectrometer configuration for the March-April 1975 field trip will be described. Many modifications have been made during the history of the instrument, so a brief description will also be given of the instrument configuration during the March 1975 and November 1974 field trips.

The last section of the chapter will discuss various tests and calibrations of the instrument, and some of the problems encountered during its operation.

History and Success of the Instrument

The spectrometer was designed and assembled in its original form by Dr. J.R. Houck, and was intended for ground based use in the atmospheric windows at 10μ and 20μ. However, it was decided that the instrument could be successfully modified for far infrared observations from the Lear Jet. These modifications commenced early in 1972, and have continued until the present. During this time almost all parts of the instrument have been completely changed, with the exception of the dewar, the spectrometer frame and the primary mirror. The process of modification has by no means

been completed, and planned future changes will be mentioned later in this chapter. The general instrument configuration during various field trips is summarized in Table 3-1 in Chapter III.

The changeover to airborne work has been quite successful. In fact, experience indicates that cooled grating instruments are probably the best solution to the problems faced during spectral observations from the Lear Jet. The major advantage of this type of instrument is its simplicity, both in structure and in operation.

The simple structure with few mechanical complexities allows the instrument to be rugged and reliable, and thus capable of withstanding both the high vibration environment of the Lear Jet and the punishment inflicted by airline baggage handlers during shipping. The simplicity of operation and data reduction makes correction for atmospheric transmission fluctuations and guiding errors much easier than in the case of multiplexing instruments, such as Fourier transform spectrometers.

The multiplexing instruments have theoretical advantages, since they can give high resolution spectra while accepting a wide bandpass. For infrared measurements, where detector noise limits the sensitivity, this gives the so-called "multiplex advantage." However, in a situation where guiding errors are important, excess noise is introduced which can greatly reduce this advantage. It is not easy to cool

these instruments because of their complexity, so high backgrounds can lead to poor detector performance.

The cooled grating instrument obtains its sensitivity by reducing the background flux on the detector. This results in improved detector performance, and sensitivity which is adequate for observing a number of sources from the Lear Jet, as is shown at the end of Chapter V.

Description of the Spectrometer

General Construction and Cryogenics

The spectrometer is a fully liquid-helium cooled grating instrument, operating in Littrow mode. It is shown schematically in Figure 2-1, and a photograph of the instrument partially disassembled appears in Figure 2-2. The frame of the instrument is all aluminum, and the spherical primary and secondary mirrors are glass, coated with aluminum and SiO. All the optical components have spring or clip mounts to avoid stress during cooling due to differential contraction. As a result, there have been few problems with breakage during cooling, and the instrument retains its alignment well.

Cooling is by conduction from the liquid helium reservoir of the dewar, and the grating and support structure reach an ultimate temperature of less than 20°K. The spectrometer is shown attached to the dewar in Figure 2-3. Dewar hold time is about six hours, more than adequate for the maximum three hour duration of a Lear mission.

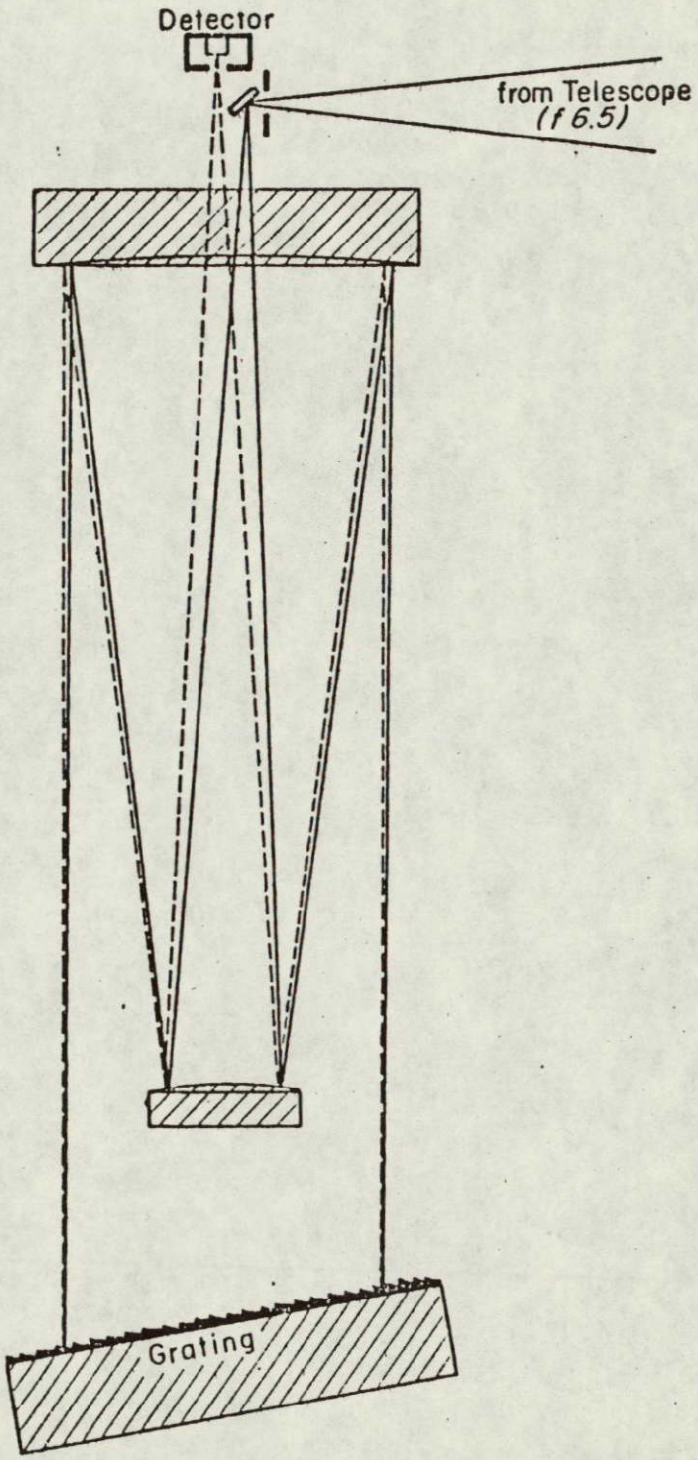

Figure 2-1. Light path in the spectrometer in the single detector configuration.

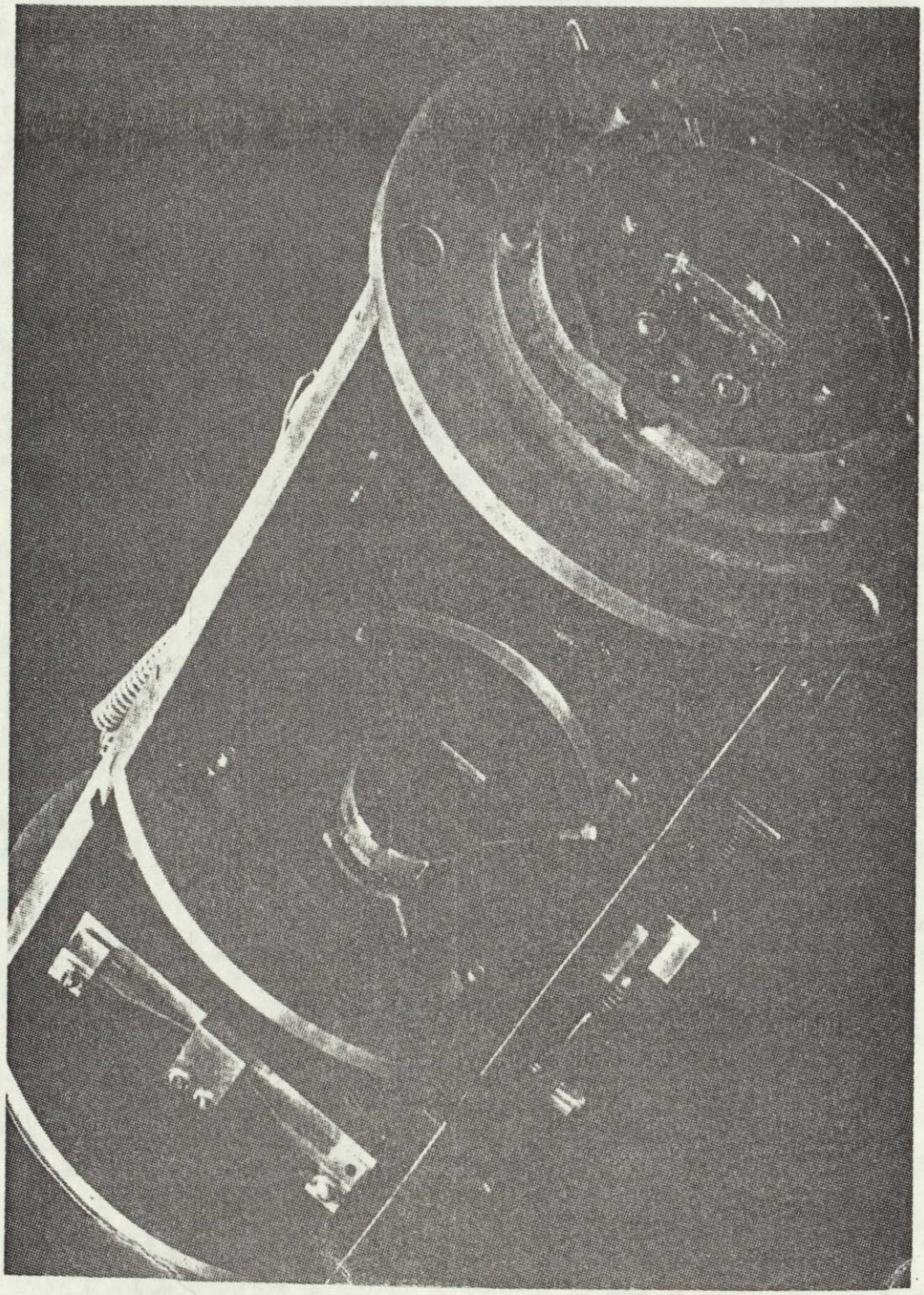

Figure 2-2. View of the inside of the spectrometer.

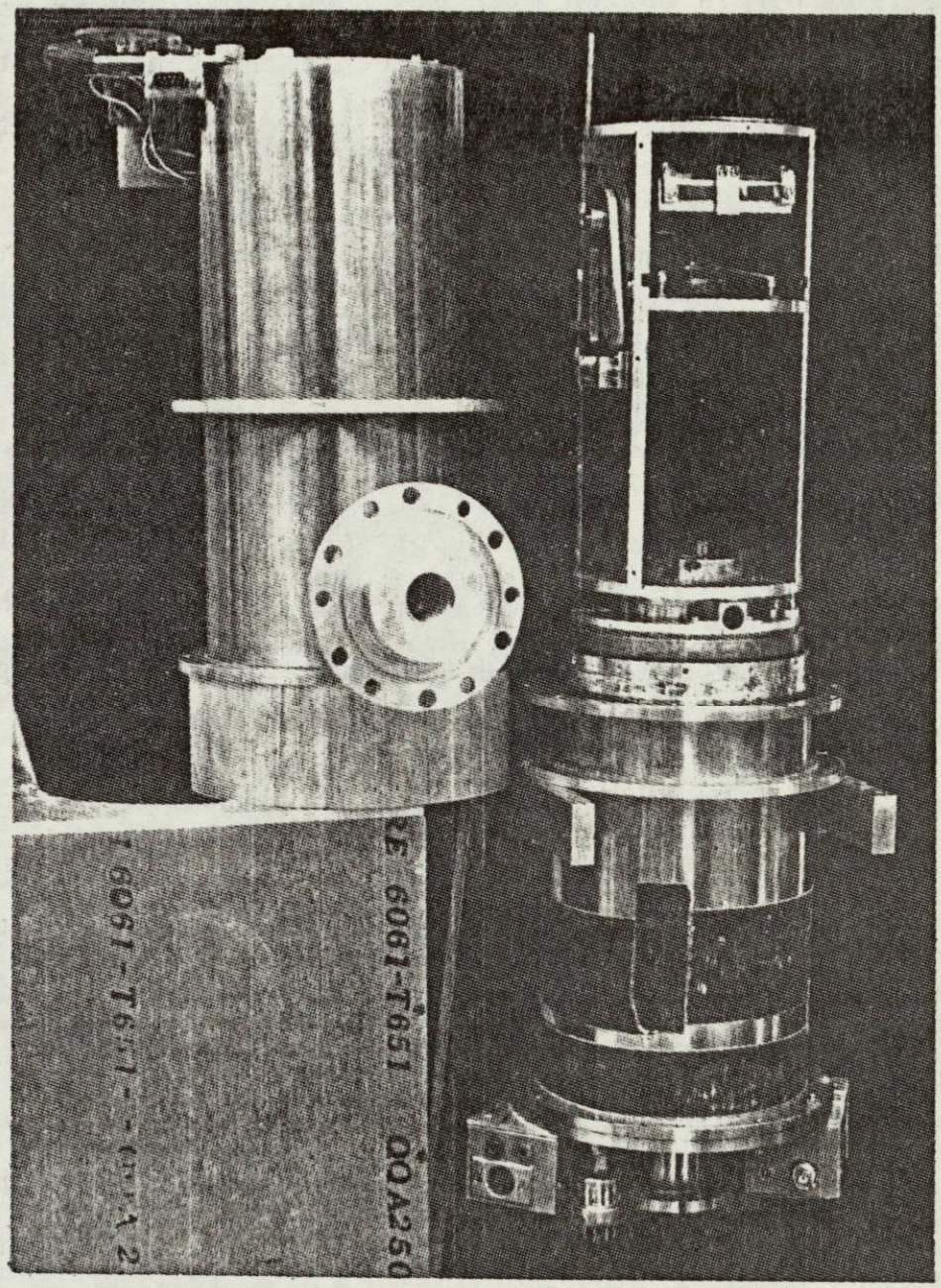

Figure 2-3. The spectrometer mounted on the dewar.

As can be seen in Figure 2-2, most of the inside of the spectrometer is coated with black paint to reduce scatter, and a black spot has been placed in the center of the secondary mirror to block the direct bounce from the entrance slit off the secondary back to the detector.

The general parameters of the spectrometer are summarized in Table 2-1.

Grating Drive and Gratings

Scanning in wavelength is accomplished by rotating the grating, which is moved by a stepping motor on the outside of the dewar. The motor drives a fiberglass shaft which goes into the dewar through a vacuum coupling and moves the grating via a gear train consisting of bevel gears, a worm, and a sector gear. The drive system is spring-loaded to reduce backlash, and is stable to less than 10% of a resolution element during a flight. The motor also drives a potentiometer whose output is used to determine the grating position.

Several interchangeable aluminum gratings are employed for observations at different resolutions. Their parameters are summarized in Table 2-2, with the resolution given being the full width at half maximum of the response to a narrow line from a Perkin Elmer 301 monochromator. Grating 1 was made on a regular milling machine, while gratings 2 and 3 were made by Lansing Research Co. on their computer controlled milling machine. The gratings are rough at optical wavelengths, but seem to work satisfactorily in the far

Table 2-1. Spectrometer Parameters.

Focal Ratio	f8
Spectrometer Focal Length	55 cm
Primary Mirror - Diameter	68 mm
- Radius of Curvature	411 mm
Secondary Mirror - Diameter	29 mm
- Radius of Curvature	210 mm
Grating Size	76 mm x 85 mm
Available Grating Angles	0 to 35 degrees
Motor Steps per Degree of Grating Rotation	425
Motor Steps per Resolution Element	∿70
Entrance Slit	2.7 mm
Exit Slits	∿3 mm
Beam Size on Lear Telescope	∿4' x 5'
Dewar Capacity	∿2 liters
Dewar Hold Time	∿6 hours
Total Spectrometer and Dewar Weight	30 lbs.

Table 2-2. Grating Parameters.

	Lines/mm	Blaze Angle	Blaze Wavelength	Spectrometer Resolution: First Order	Spectrometer Resolution: Second Order
Grating 1	1.33	3.8°	100μ	∿4.5μ	∿2.3μ
Grating 2	0.53	1.53°	100μ	∿11μ	∿5.5μ
Grating 3	3.94	11.3°	100μ	∿1.4μ	∿0.7μ

infrared, although their efficiency has not been determined.

Filters and Detectors

The filter and detector mounts are shown in Figure 2-4. A scatter-coated CaF_2 filter (Armstrong and Low, 1973) in the filter mount marked number 4 at the entrance to the spectrometer cuts off radiation shortward of 40μ. This filter has a small leak in the visible portion of the spectrum, but the gratings are very rough at optical wavelengths, and act as a scatter filter for the optical light which gets through. The other filters are normally mounted on the spectrometer detector blocks marked 1 and 2 to sort orders for long wavelength (70μ - 115μ) or short wavelength (40μ - 80μ) observations. The filter used at long wavelength is a Yoshinaga filter constructed by Dr. J. Pipher, and cuts off radiation shortward of 60μ. It turns on rather slowly, reaching maximum transmission at wavelengths beyond 90μ. The short wavelength filter is KRS-5, antireflection coated with polyethylene. This filter cuts off light at wavelengths longward of 82μ. It was purchased from Infrared Laboratories, Inc., as was the scatter-coated CaF_2 filter.

The two spectrometer detectors are Ge:Ga photoconductors (Moore and Shenker, 1965; Pipher, 1971). They view the light coming out of the spectrometer, off the aluminum 45° mirrors, and through the exit slits and filters into the detector blocks. Their separation is 1.3 resolution elements along

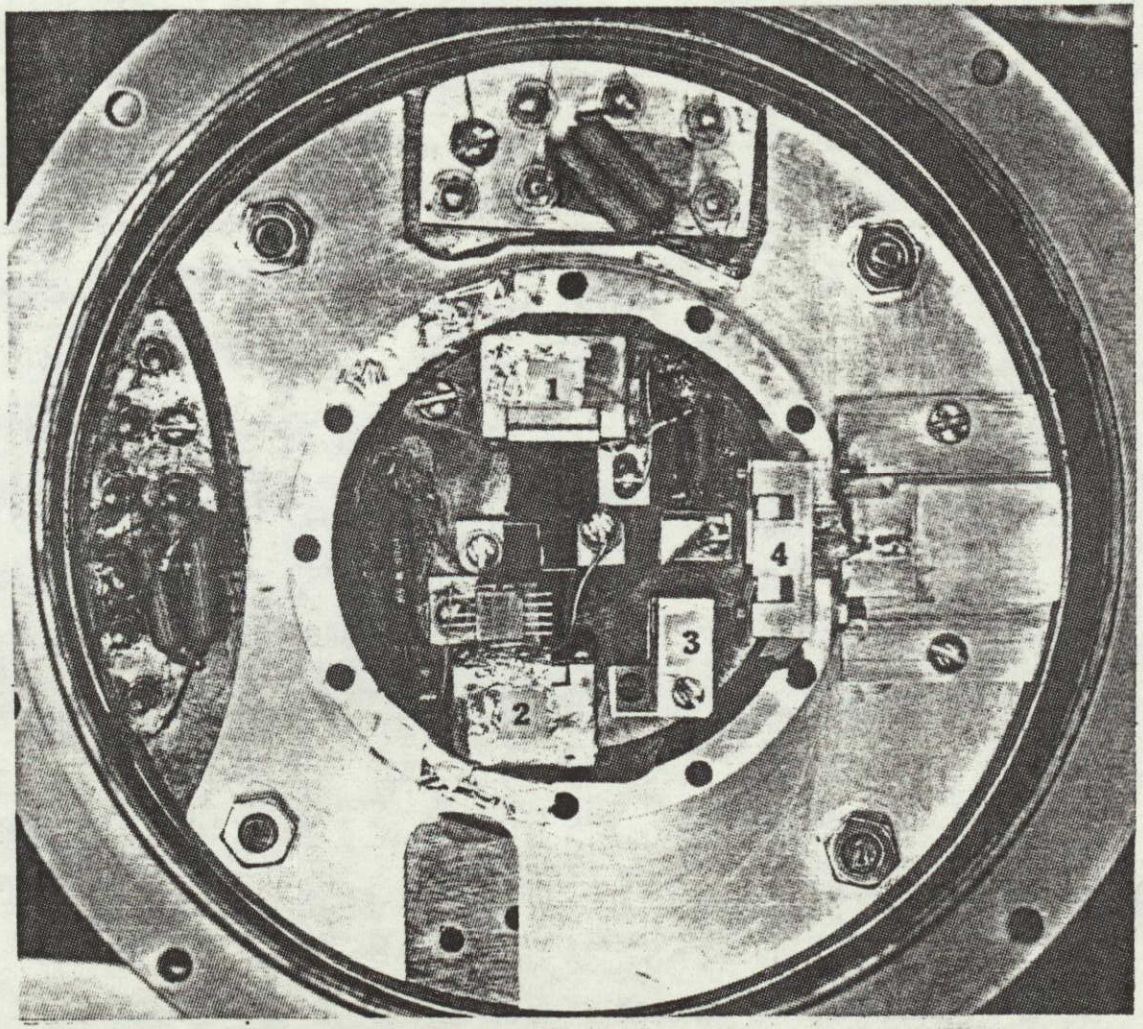

Figure 2-4. The detector blocks, preamplifiers and filter mounts.

the direction of dispersion, and they are lined up so that they receive light from the same part of the entrance slit. The long wavelength detector has a system NEP (Noise Equivalent Power) of $\sim 1.5 \times 10^{-12}$ watts-Hz$^{-0.5}$ at 95μ, and the short wavelength NEP is $\sim 5 \times 10^{-12}$ watts-Hz$^{-0.5}$ at 55μ. These values are determined from the signal to noise ratio during coarse resolution observations of M17 and M42. The limiting factors are thought to be detector noise and light losses in the spectrometer.

A third Ge:Ga detector is mounted in detector block number 3. It views light in the range from 40μ out to the detector response cutoff at about 130μ. This detector is used as a "finder" for weak sources, particularly those with no optical counterpart. It detects radiation coming from the telescope which otherwise would focus just below the entrance slit of the spectrometer. Once the source is located with this detector, the observer can offset so that the source will be imaged on the spectrometer entrance slit.

The detectors are all glued with GE 7031 varnish to a large copper disc which is fastened directly to the copper bottom of the helium reservoir. This ensures that they are all at their operating temperature of 4.2°K.

Preamplifiers

Under observing conditions, the spectrometer detector impedances are close to 10^9 ohms. Hence a large cooled

bias resistor (10^9 ohms) is used, in order to get reasonable signal levels. A cooled metal-oxide-semiconductor field effect transistor (MOSFET) source follower is used as an impedance transformer, and is connected to a junction field effect transistor (JFET) amplifier on the outside of the dewar. The bias resistor and the MOSFET are mounted as close as possible to the detector, to minimize stray capacitances. The circuit is shown in Figure 2-5. The DC output of the source follower can be used to calculate the DC impedance of the detector, using the formula

$$R_D = \Delta V\left(\frac{R_L}{GV_R - \Delta V}\right)$$

where ΔV is the change in DC output of the source follower when the bias is turned on, V_B is the bias voltage, R_L is the bias resistance, and G is the DC gain of the MOSFET (about 0.75 in this case).

The finder detector impedance is much lower, and it is coupled to a cooled 3 megohm load resistor and a JFET preamplifier which is located outside the dewar.

Instrument Configuration--Earlier Flight Series

The major difference between the present instrument configuration and that employed during earlier field trips is that the earlier observations were carried out using only one detector. In both March 1974 and November 1974 observations were made from 75 to 120 microns only.

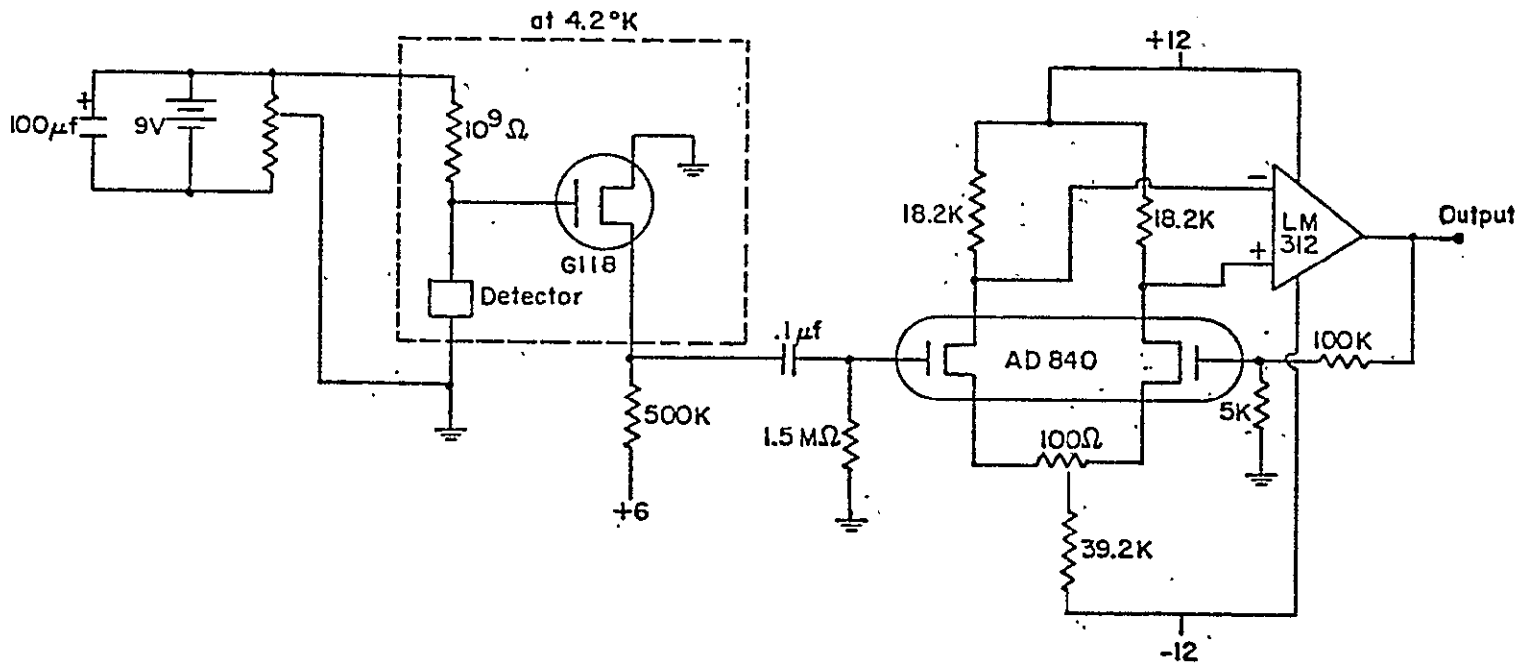

Figure 2-5. Schematic for the preamplifier.

Different preamplifiers were used as well. In March 1974 an Ithaco Model 144 preamplifier was mounted in a box strapped to the outside of the dewar. This arrangement proved to be very susceptible to microphonic pickup in the high vibration environment inside the Lear Jet, so a JFET preamplifier was built which mounted directly to the connector on the top of the dewar. It is this preamplifier which is the second stage in the present preamplifier system. Marked improvement in the amount of microphonic pickup was noted during the November 1974 flight series, but the problem was still troublesome. The present MOSFET preamplifiers seem to have eliminated the problem entirely.

Instrumental Tests and Calibrations

Wavelength Calibration

The wavelength calibration was obtained from water vapor features in the atmospheric transmission spectrum. The transmission spectrum expected at typical flight altitudes is shown in Figure 2-6. It was calculated at 0.2μ resolution with 5 precipitable microns of water along the line of sight. Data on water vapor line parameters was obtained from McClatchey et al. (1973).

There are many features in the transmission spectrum which can be used directly for calibration at high resolution. At low resolution these features smear out. However, one can increase the spectrometer resolving power by narrowing

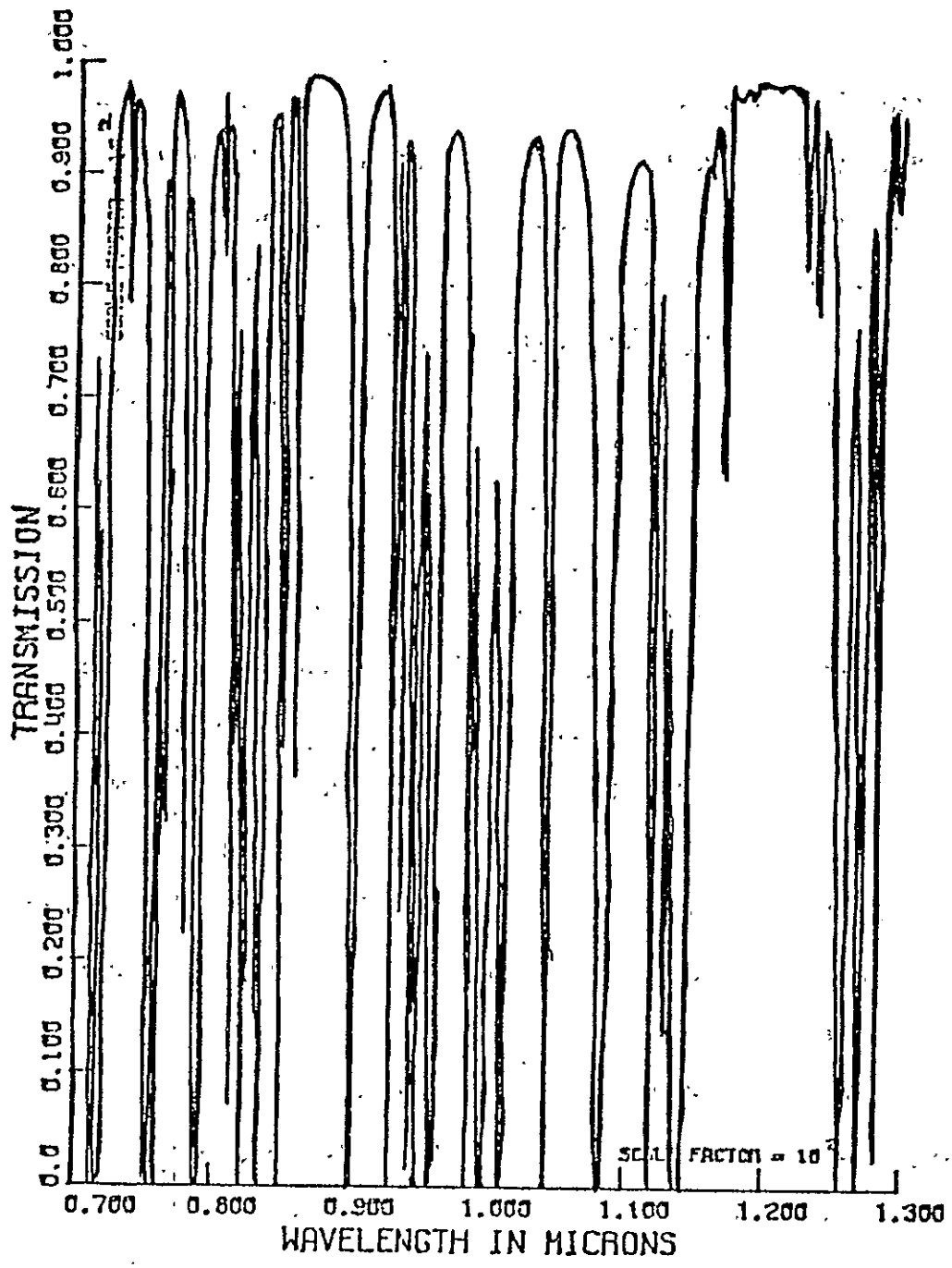

Figure 2-6. Calculated atmospheric transmission from 14 km altitude, assuming 5 precipitable microns of water along the line of sight. The transmission was calculated at 0.2μ resolution using water vapor line data from McClatchey et al. (1973).

the slits, then observe the resulting spectrum and zero order during the same spectral run. The wavelength calibration thus determined relative to zero order can be used for calibrating spectra taken with slits at their normal width. There is some error introduced by changes in effective wavelength, but these changes are not large. A check can be made by calculation using the design parameters for the grating. For the coarse resolution gratings these two approaches agreed very closely.

Resolution

The instrument resolution was tested using a Perkin Elmer spectrometer as a monochromatic beam source. The Perkin Elmer was set to give a beam at a given wavelength, and the spectrometer was then scanned through that wavelength in small steps. When the "line" output of the Perkin Elmer was much narrower than the resolution of the spectrometer, the resulting signal output gave a good measure of the spectrometer resolution.

The results for coarse resolution and high resolution gratings are shown in Figure 2-7 for the long wavelength detector. The width in grating steps can be converted to wavelength by using the grating characteristics given in Table 2-2 and the spectrometer parameters given in Table 2-1, and give the resolutions quoted in Table 2-2.

Unfortunately, there is evidence that the resolution of the instrument is dependent on whether the source of radiation

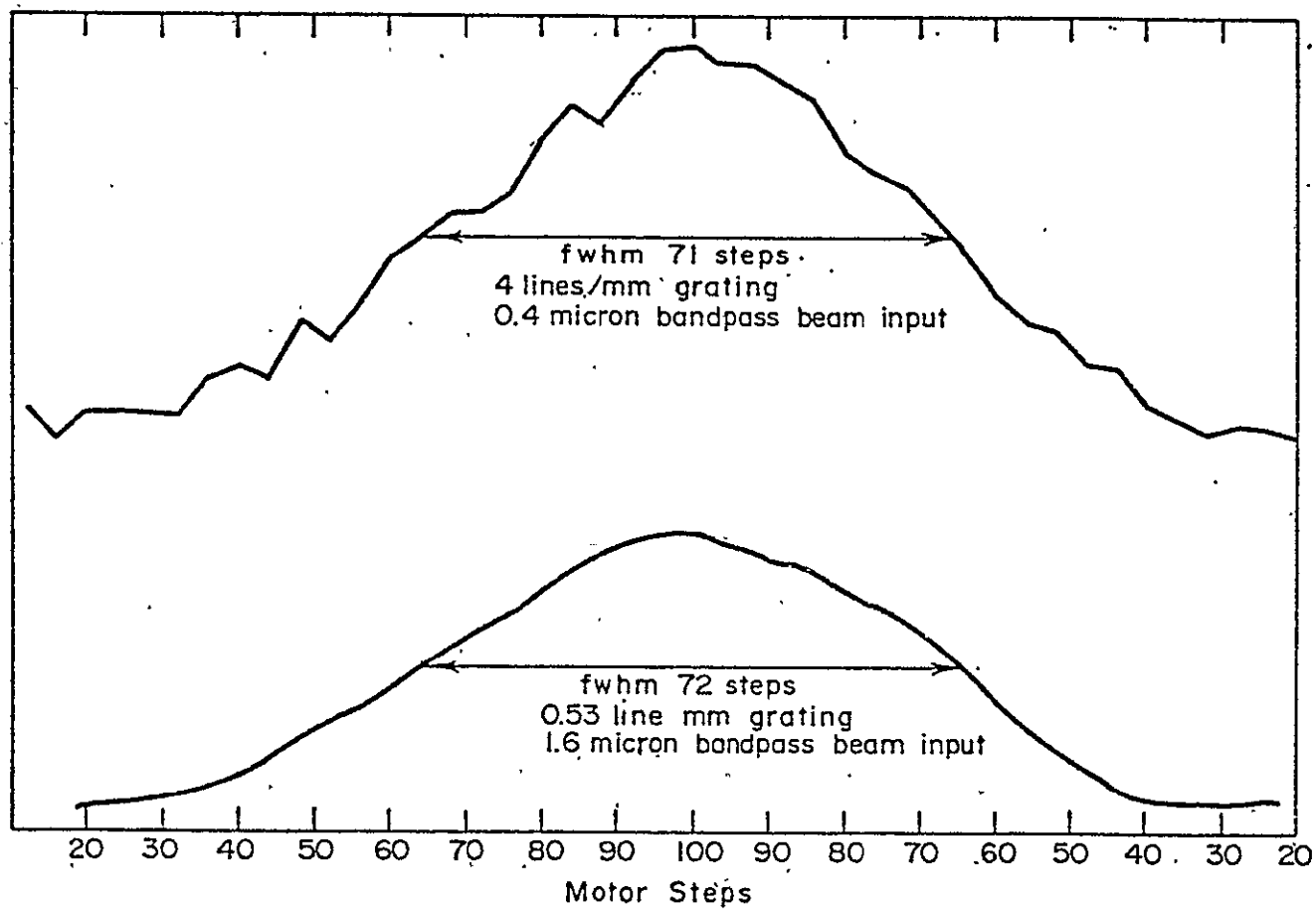

Figure 2-7. Resolution tests--the response of the spectrometer scanning through a line output from the Perkin Elmer 301.

illuminates all of the entrance slit. Observations of the moon (which uniformly fills the entrance slit) yield shallower atmospheric transmission features than observations of planets or H II regions.

This effect may be produced in laboratory tests as well. Figure 2-8 shows a comparison of the atmospheric transmission features in the lab for 1 mm and 2.7 mm entrance slits, with 3 mm exit slits in both cases. Several small features show up in the 1 mm slit spectrum but not in the spectrum at normal slit size.

During the laboratory measurements of the instrumental resolution, the entrance slit is fully illuminated, so the measured bandpass is again somewhat larger than the bandpass for observations of H II regions or planets. To correct for this effect, in the high resolution results presented in Chapter IV the instrumental bandpass has been taken to be 10% smaller than what is measured using the Perkin Elmer 301.

The probable cause for this effect is uneven response across the exit slit. The results of zero order scans tend to lend weight to this interpretation. In zero order the grating acts as a mirror for all wavelengths. Hence if the exit slit has even response across all of its width, the half power width of the zero order signal should be roughly independent of the entrance slit width as long as the entrance slit width is less than that of the exit slit. However, as seen in Figure 2-9, the half width is significantly narrower

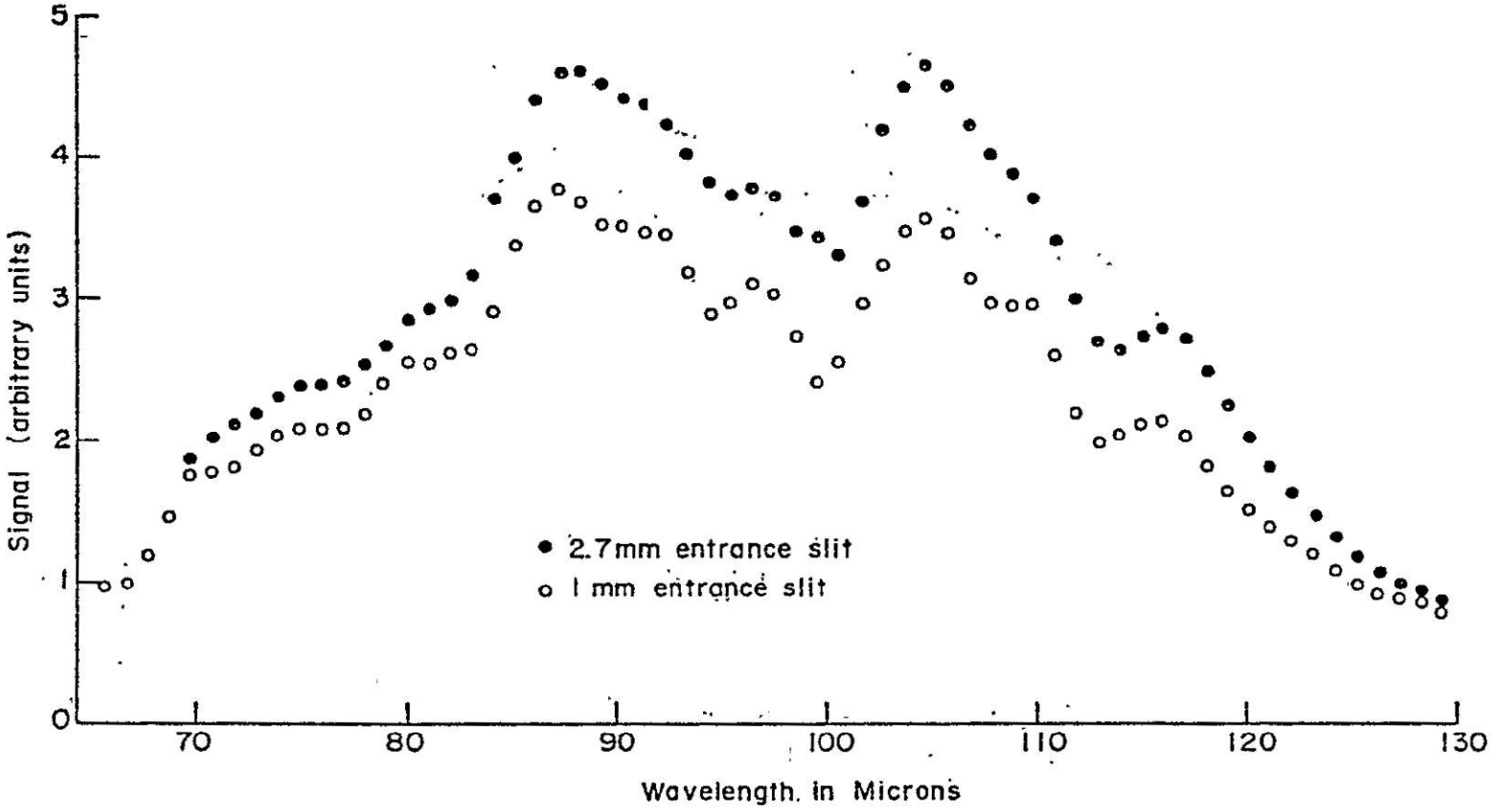

Figure 2-8. Illustration of resolution changes as a function of the entrance slit size. Liquid nitrogen was used as a source, and the features are water vapor lines.

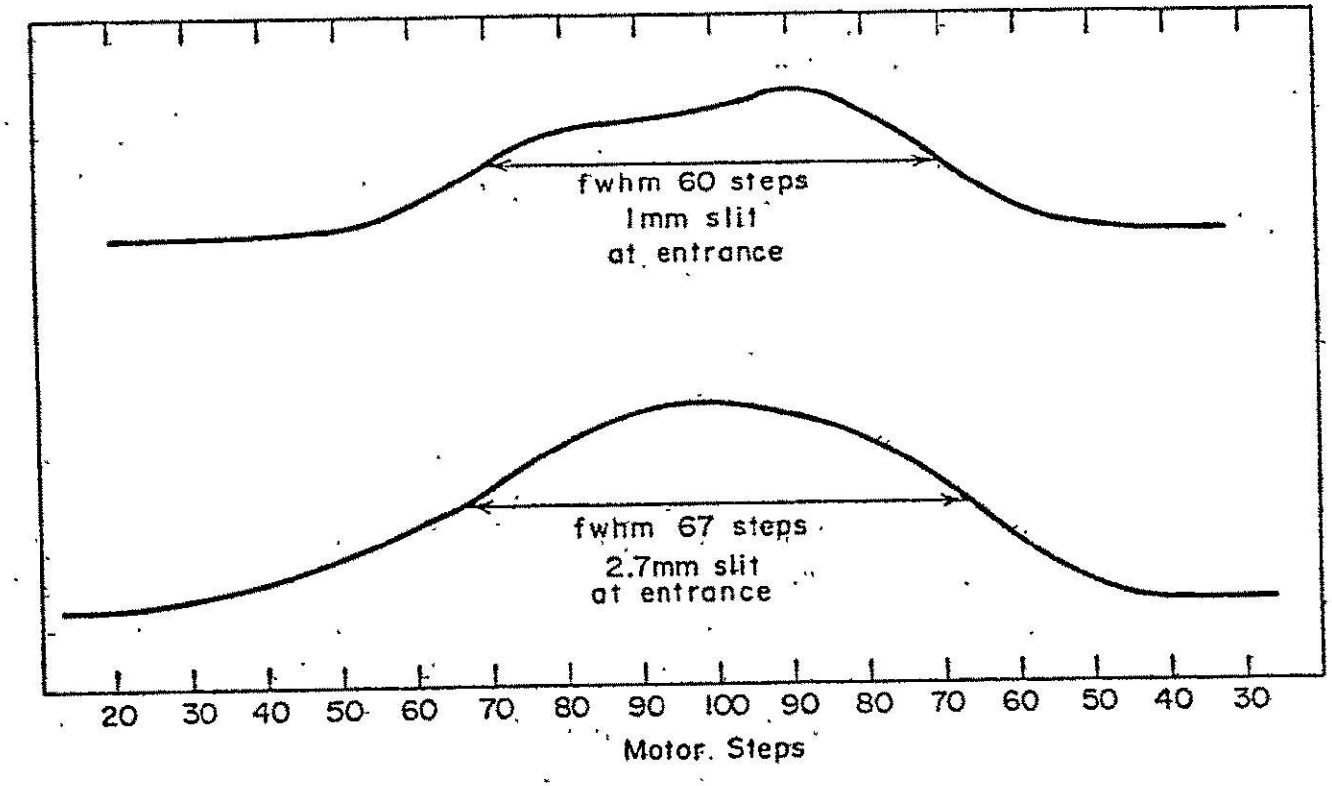

Figure 2-9. Zero order scans for different entrance slits.

for the narrow entrance slit, and shows a rather asymmetric shape.

One possible cause for the problem could be uneven response across the detector. This could occur if the integrating sphere worked better for light coming through some parts of the exit slit than for other parts. In Ge:Cu detectors it is found that response will vary across the surface of the detector itself (Forrest, 1975). If a similar effect exists for Ge:Ga it would tend to give the results which are observed.

A second cause for the uneven response may be defocussing of the light after the exit slit. The detector is roughly the same size as the exit slit, and is about half an inch away. Thus some of the light which focusses very near the edge of the slit may miss the detector. It is not clear how important this effect will be since some of the light still ends up in the integrating sphere and may hit the detector on the first bounce. The Lear Jet telescope focus is very rough at the best of times, due apparently to a badly figured primary mirror, and defocussing due to this may also play a part in the situation during actual observations.

At any rate, this effect makes calibration with the moon less satisfactory, as will be pointed out in the discussion of the data in later chapters.

Beam Shape Determination

Knowledge of the beam shape is important for analysis of observations of extended sources. The most satisfying method of determining the beam would be to observe a strong point source from the Lear Jet and drift through it from various angles. Unfortunately the guiding accuracy of the Lear Jet telescope is sufficiently bad to make this approach rather difficult.

As a result, all the information concerning the beam has been derived from laboratory measurements, using an optical bench as an telescope, and viewing chopped infrared signal through a pinhole. The beam profile obtained is shown in Figure 2-10. This beam profile was obtained with the spectrometer set on the atmospheric transmission peak at 87μ, using the 0.53 lines/mm grating.

It can be seen that the beam has a half power width of about 2.9 mm along the length of the slit and 2.2 mm along the direction of disperson. On the Lear telescope this corresponds to a beam of roughly 4' x 5'. The beam is relatively flat in the laboratory measurements, but in the air the response seems to have a sharper peak. Moving a source like Venus even one arc minute in the beam will produce important changes in signal level.

A flatter beam would assist greatly in improving the observational data. Guiding noise has been the major source of error in the data up to the present, and a flatter beam

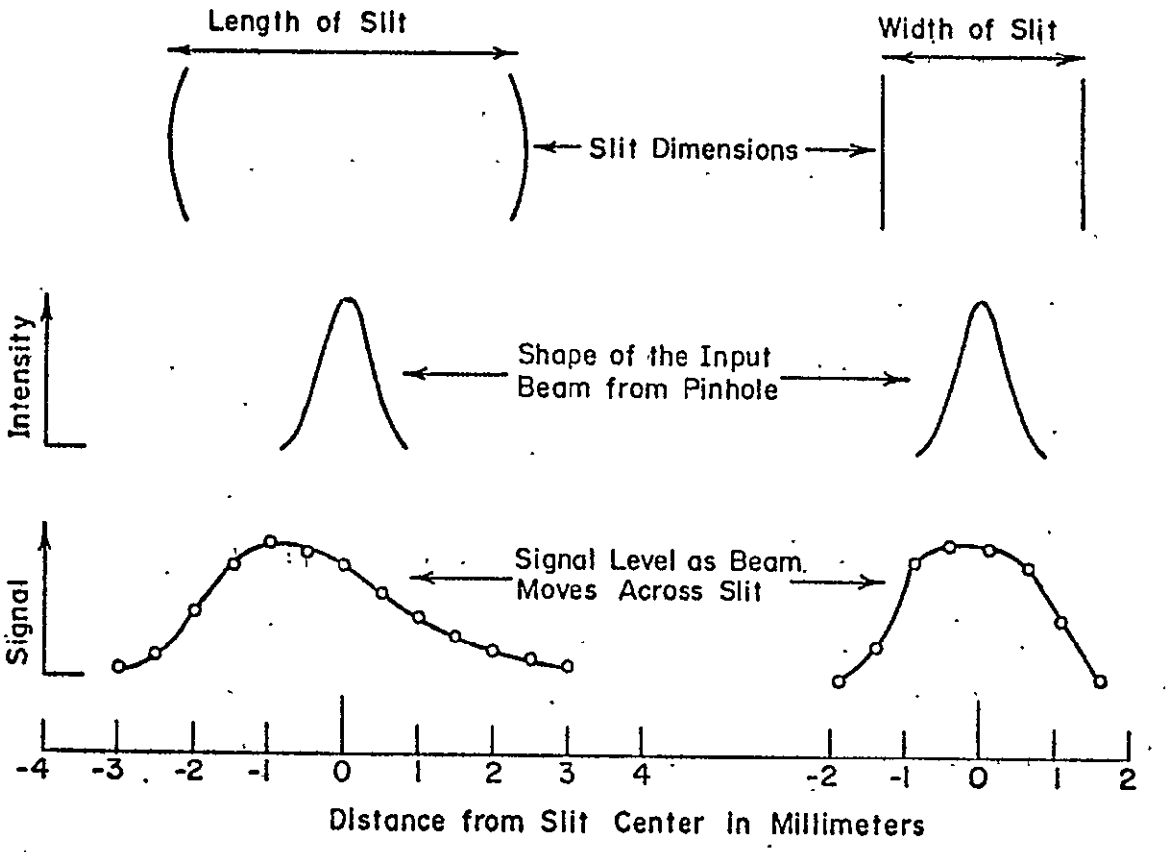

Figure 2-10. Beam profile, scanned along the width (direction of dispersion) and length of the slit.

would assist in reduction of this noise component, particularly in observations of planets.

Linearity

This subsection will deal with a problem that affects the coarse resolution data from the March-April 1975 field trip. It was found that the output signal level from the spectrometer for a given amount of signal power on the detector was strongly dependent on the background at which the detector was operating. Here the background is defined as the total radiant power incident on the detector. Thus moon calibration spectra looked quite different from H II region spectra, simply because the moon was so bright that it radically changed the background level at the detector.

To understand why this problem arose in the recent data, consider the typical preamplifier and detector circuit shown in Figure 2-11. If the flux of photons on the detector changes by ΔI, the resistance of the detector changes from R_D to $R_D - \Delta R$, and the voltage change at the preamplifier input is

$$\Delta V = V\left[\frac{R_D}{R_D + R_L} - \frac{R_D + \Delta R}{R_D - \Delta R + R_L}\right]$$

$$= V\left[\frac{R_L \, \Delta R}{(R_D + R_L)(R_D + R_L - \Delta R)}\right]$$

In earlier field trips $R_L << R_D$. Also $\Delta R << R_D$ was generally true even for moon observations, because of

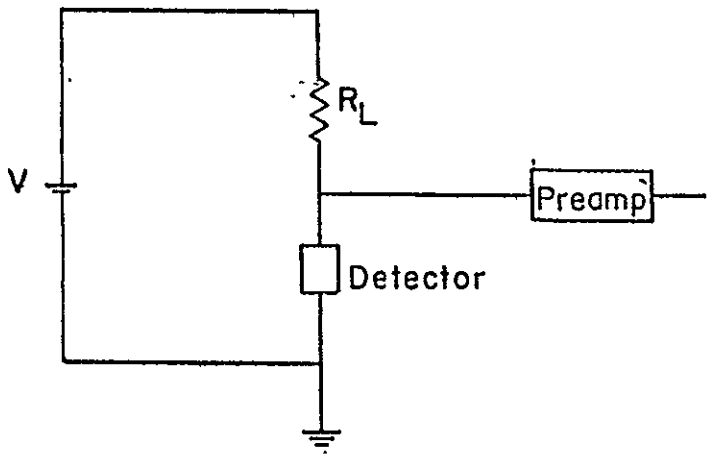

Figure 2-11. Basic detector bias and preamplifier circuit.

relatively high background levels within the instrument itself. Therefore the above expression reduced to

$$\Delta V = \frac{V R_L \Delta R}{R_D^2}$$

For photoconductors, in this small signal limit

$$\Delta G_D = \gamma \Delta I$$

where γ is a constant, and ΔG_D is the conductance change of the detector.

But

$$\Delta G_D = \frac{-\Delta R}{R_D^2}$$

and so

$$\Delta R = -\gamma \Delta I R_D^2$$

and

$$\Delta V = -V \gamma \Delta I R_L$$

which does not depend on the detector resistance, and therefore does not depend on the background.

However, in the system used during the March-April 1975

field trip, R_D and R_L are of the same order of magnitude. Furthermore, $\Delta R << R_D$ was no longer true for moon observations, since better filter cooling and detector baffling have decreased the normal background on the detector. Hence system sensitivity was different during lunar observations than during observations of other sources, particularly for the short wavelength band from 40μ to 80μ.

Laboratory measurements of the sensitivity as a function of background were made by clamping a soldering iron in front of a source of chopped infrared emission so that the background flux could be changed by heating up the soldering iron, while maintaining a constant signal flux from the infrared source. The signal level and the detector resistance were recorded at the usual grating positions covering the available bandpass, with the soldering iron turned off. Then the soldering iron was heated up and the process repeated. The information derived was used to plot Figures 2-12 and 2-13. These figures are by no means accurate, but give a general idea of the magnitude of the effect.

In the figures, a sensitivity of 1 corresponds to the sensitivity of the detector per signal photon under the lowest possible background flux. This lowest background occurs when the spectrometer is set for a wavelength far off the passband of the filters. As the grating is turned and the detector begins to see light coming through the filters, the background goes up and the signal output from the detector

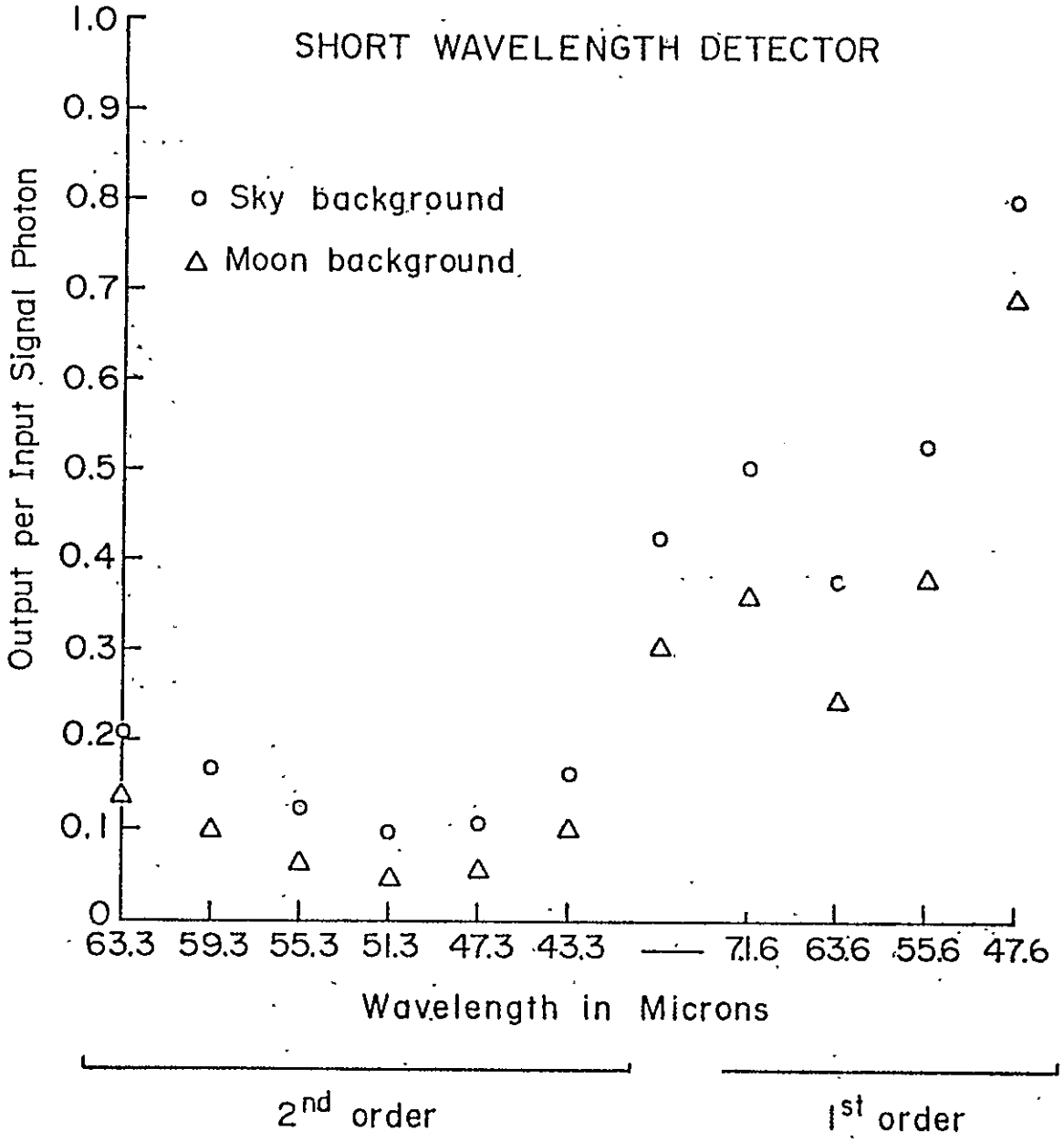

Figure 2-12. Short wavelength detector--voltage output per unit signal photon reaching the detector, as a function of background at normal grating positions. A value of 1 corresponds to the response at the internal background of the spectrometer, as described in subsection on linearity.

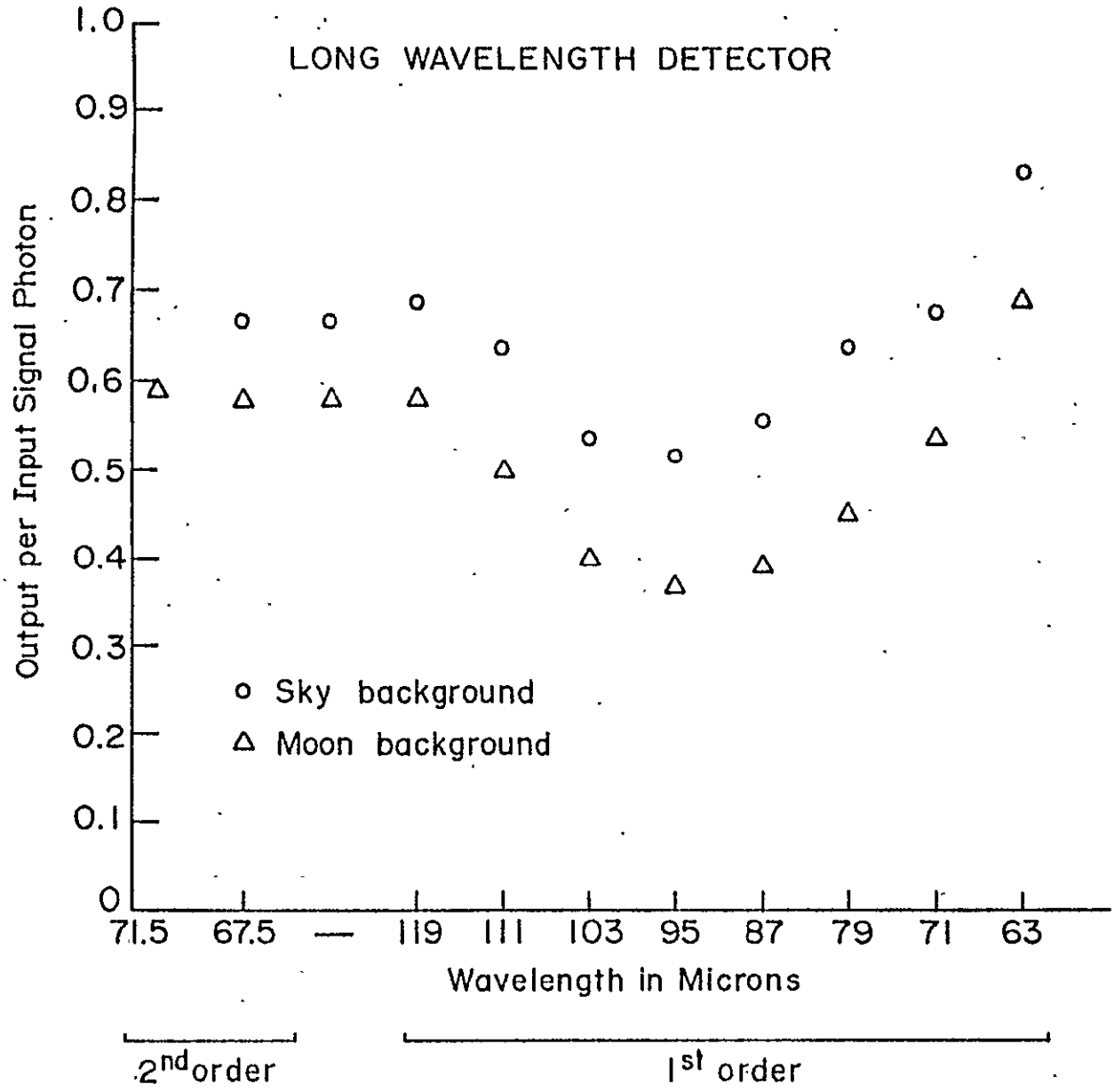

Figure 2-13. Long wavelength detector--voltage output per unit signal photon reaching the detector, as a function of background at normal grating positions. A value of 1 corresponds to the response at the internal background of the spectrometer, as described in subsection on linearity.

per signal photon goes down. In the graphs of Figures 2-12 and 2-13, the sensitivity per signal photon is shown for the cases where the instrument is looking at the sky and looking at the moon. There is a marked difference in the response in the two cases.

In theory, it would be possible to calibrate out this effect using measurements of the detector resistance to monitor background changes. However, these are DC measurements, and drifts introduced so much error that the calibration with the moon was very inaccurate.

Fortunately, during flight the background levels were roughly the same from night to night, as shown by the fact that signal levels were reproducible and spectra very similar. Thus the data were still useful, as will be shown in Chapter V. However, it would be much better not to have to worry about possible background changes. Hence efforts will be made in the future to get back to the performance typical of the small load resistor case. A circuit using an operational amplifier has been used successfully (Schaack, 1975) for this purpose, while retaining the large bias resistor. However, since $\Delta R << R_D$ no longer holds during lunar observations, moon calibrations still may be unsatisfactory. Future calibrations will probably have to be done with observations of Mars or other planets.

Scattered Light

Scattered light in the instrument has always been a

problem. Most of the interior of the instrument is painted black in an attempt to absorb scattered light, but a baseline still appears as one can see in Figure 2-14 below 60μ. This figure is from the November, 1974 field trip, when the scatter levels were quite high. The baseline in the other field trips was always less than 10% of the average signal for coarse resolution lunar observations. In the reduction of the data this baseline must be subtracted from the raw results.

Fortunately the scatter level appears to be independent of the grating orientation, so such a general subtraction probably does not introduce any major errors. Evidence for this lack of dependence on grating angle comes from the scans of zero order, and from the scans of a line input from the Perkin Elmer 301 monochromator during resolution tests. In both cases only one peak is seen, with a flat baseline on both sides form the scatter contribution.

The scatter is still an irritating problem, however, as the scatter level must be determined in order to make the subtraction correctly. During observations of H II regions this level has in general not been well determined. For the November 1974 results this is an important problem, as the scatter contribution is quite large due to the black spot having fallen off the secondary mirror of the spectrometer. The spectrum shown in Figure 2-14 has a high scatter level partly for this reason, and partly because it is a high

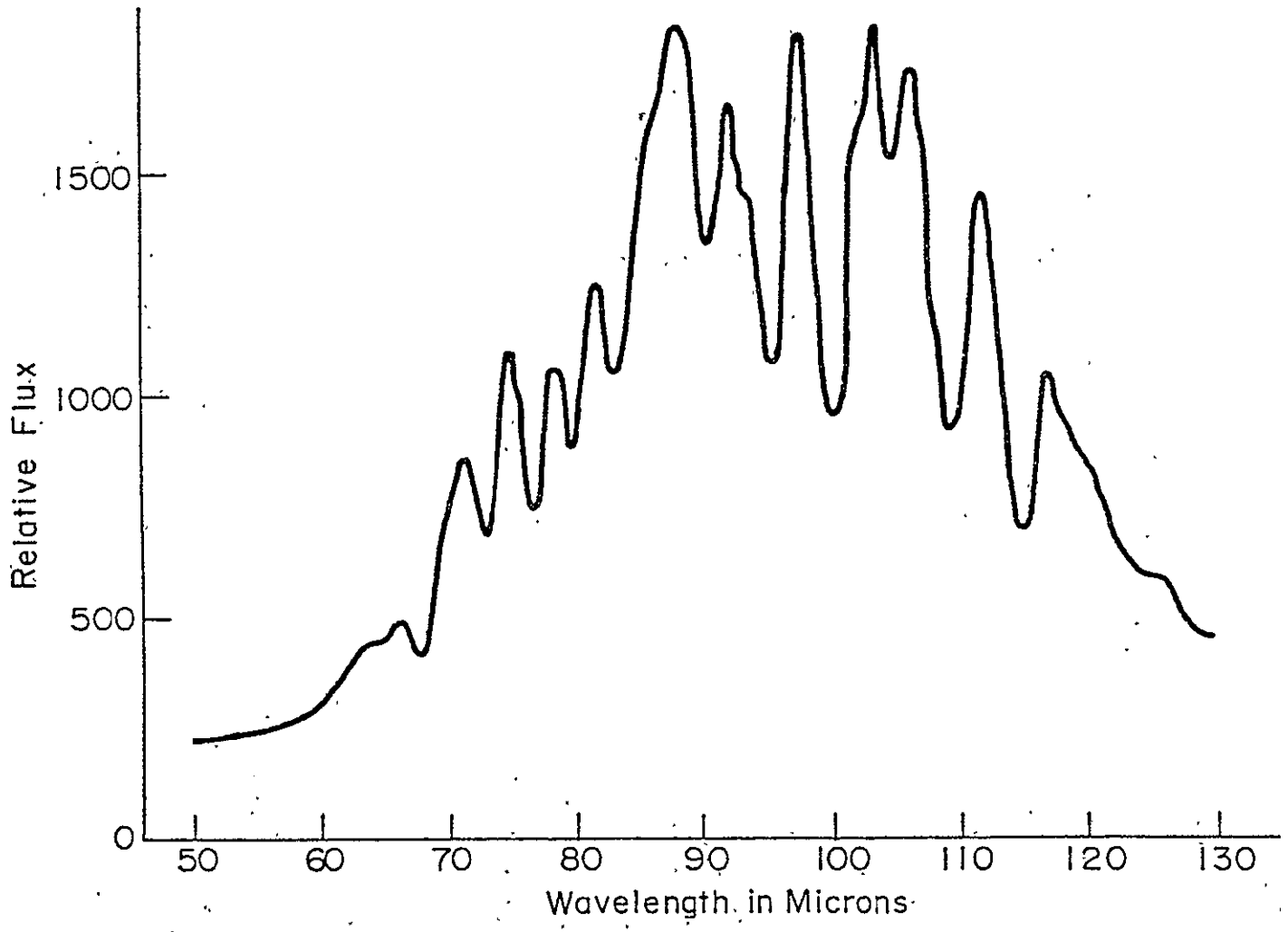

Figure 2-14. Uncorrected lunar spectrum of 1.45μ bandpass from the November 1974 field trip. Features are due to atmospheric water vapor. Random errors are too small to plot.

resolution spectrum. The scatter signal level is pretty much independent of the instrumental resolution, so for lower resolution data (where signal levels are higher) the relative scatter level is lower, but still may be important at grating positions where signal is low. This is part of the reason why information from such grating positions has usually not been used in the spectra shown in Chapter V. This will be discussed in the following subsection.

Sensivity as a Function of Wavelength

The instrumental sensitivity as a function of wavelength is shown in Figure 2-15. This has been determined from the calibration corrections in the April 1975 flight series, and hence some atmospheric effects are present as well (since the offset was used for that calibration) but should not be important because of the coarse resolution, which tends to smear them out.

The instrumental sensitivity decreases steadily toward shorter wavelengths. This is partly due to the decrease in detector sensitivity toward shorter wavelengths, as shown by Moore and Shenker (1965) in the original paper on Ge:Ga detectors. However, other effects are present as well.

For the long wavelength detector, the filter begins to cut off below 85μ. The efficiency of the grating also decreases rapidly below 75μ. The point at 63μ has not been used in the final results, because the signal level there is very low, making this point subject to systematic errors

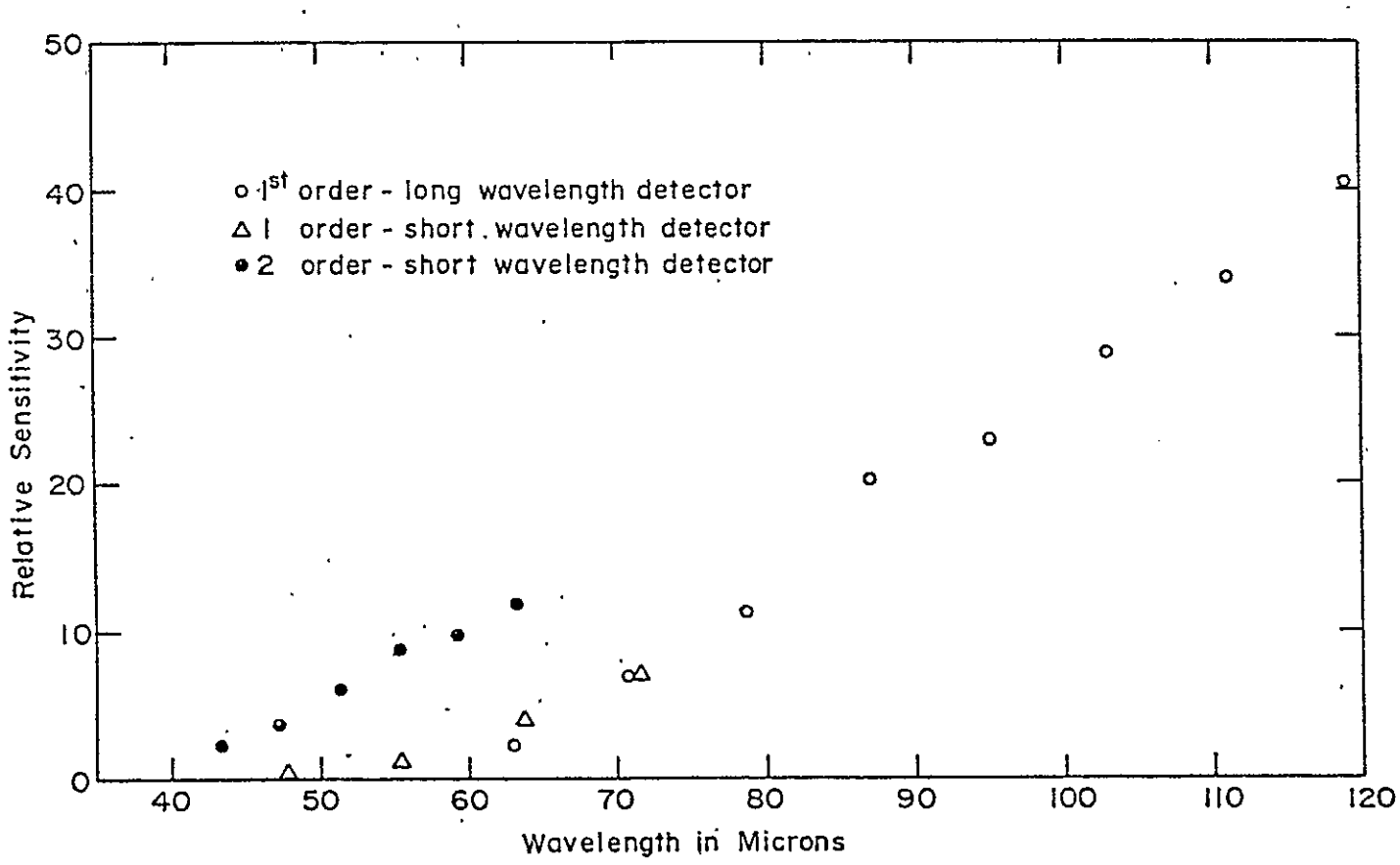

Figure 2-15. Overall relative sensitivity of the spectrometer as a function of wavelength during the March-April 1975 observations.

in the scatter correction. At long wavelengths, points above 115μ have not been used in the March-April 1975 data because of low signal levels and possible contamination from second order. Points were taken in second order at 67.5μ and 71.5μ (not shown in the figure), but again signal was low and there was a possibility of some contamination from first order.

The short wavelength detector was used mainly in second order, where the sensitivity decreases steadily toward shorter wavelengths, partly due to the filter starting to cut off below 50μ. The point at 43.3μ was not used, because of low signal levels. In first order, only the point at 71.6μ was used. The grating efficiency decreases rapidly after that, and signal levels again are quite low. The grating position at 63.3μ suffers somewhat from contamination from third order at 42μ. However, it was still used in the final results since not much is expected to come through from third order because the filter is cutting off and the grating efficiency is probably quite low.

One of the major problems of the spectrometer in its present form is illustrated by this sensitivity graph. The sensitivity is quite poor between 63μ and 80μ, and there is not much overlap between the two detectors. Thus the results depend on the calibration to make the fit between the spectral ranges of the two detectors, and if the calibration is not good, the spectrum cannot be tied together with much confidence.

In the future a grating blazed at 75μ will likely be used, to increase the grating efficiency in the troublesome 65μ to 80μ region. Also, a BaF_2 restrahlen filter will be used on the long wavelength detector, for better transmission below 80μ, with the filter cut-off still at 60μ.

Filter Tests

Filter tests were carried out to check for leaks outside the desired passband of the filters. For the old filter system used in early field trips, leaks were not a problem. Putting a filter in front of the instrument which blocked radiation longward of 60μ would reduce the signal to negligible levels.

However, the new filter system used in the last flight series in March-April 1975 had an optical leak. Fortunately this leak was quite small, and the gratings are sufficiently rough at optical wavelengths to be good scatter filters. Thus the optical leak may have increased the scatter baseline slightly, but had no other effect. This was tested by putting a bright optical lamp and a chopper in front of the dewar and using glass to block the far infrared signal. The resulting signal followed the sensitivity dependence of Figures 2-12 and 2-13, showing that a constant number of visible photons were reaching the detector, independent of the grating orientation.

In the future, black polyethylene of some other short wavelength filter will be used to block optical photons completely.

CHAPTER III

OBSERVING PROCEDURE AND DATA ANALYSIS

In this chapter, I will give a general description of the observations and data analysis. In the presentation of the results in Chapters IV and V, any special problems or divergences from the usual observing routine will be discussed in the context of the observational data.

Field Trips

The observations were carried out from the NASA Lear Jet, which is based at Ames Research Center in California. As a result, each observing series necessitated a field trip of at least two weeks duration. There have been a total of six field trips in all, and these are summarized in Table 3-1.

The recent field trips have all been during the period between October 15th and June 1st, since the tropopause is often at altitudes above 14 km during the summer months, and water vapor absorption becomes strong and variable.

The Lear Jet Telescope

In order to give a background for the discussion of observing procedure and data analysis to follow, I will now

Table 3-1. Field Trips.

Date	Duration	Flights	Type of Detector	Available Bandpass	Observers	Comments
September 1972	3 weeks	3	Ge:Cu	18- 25μ	C. Frederick L. King D. Ward	Telescope gyros failed, no useful data was obtained.
January 1973	2 weeks	5	Ge:Cu	18- 25μ	M. Jacobson D. Ward	Spectrometer problems--secondary mirror fell off. No useful data.
August 1973	2 weeks	9	Ge:Ga	70-120μ	M. Jacobson M. Harwit D. Ward	Obtained spectra of Jupiter and moon. Lot of water vapor--could not calibrate.
March 1974	3 weeks	12	Ge:Ga	70-120μ	D. Briotta M. Harwit D. Ward	Obtained spectra of M42 and Venus. First useful data.
November 1974	3 weeks	16	Ge:Ga	70-120μ	B. Dennison G. Gull M. Harwit D. Ward	Spectra of Jupiter and M42. Searched for (O III) 88.16μ in M42.
March-April 1975	7 weeks	18	Ge:Ga	45-115μ	B. Dennison G. Gull M. Harwit D. Ward	Coarse resolution spectra of M42, M17 and Venus. Detected (O III) 88.16μ in M17.

give a brief description of the Lear Jet telescope, which has been built and is maintained by the infrared group at NASA Ames (Erickson et al., 1974).

The telescope is a 30-cm aperture Cassegrain with Dall-Kirkham optics, and is very similar to the telescope described by Low et al. (1970). It is shown in Figure 3-1 as seen from the inside of the aircraft. The telescope is gyrostabilized, but the pointing must still be controlled by the observer who guides the telescope with a joystick while looking through the finder telescope attached to the side of the main telescope. The accuracy of the pointing is dependent on a number of factors, including the smoothness of the flight and the weight of the instrument. The spectrometer is relatively heavy, and so guiding accuracy is limited to about one arc minute under good conditions.

Chopping the input photon flux is necessary because of the large atmospheric signal, many times the typical source strength. The source is chopped against the sky by an oscillating secondary mirror, which was normally set to have a throw of from ten to fifteen arc minutes. The brightest portions of sources we have observed are much less than ten arc minutes in extent, judging from published 100μ maps (Fazio et al., 1974; Werner et al., 1975; Harper et al., 1975), so with a five minute beam one is confident that one is indeed chopping on and off the source.

The Lear telescope points out the side of the aircraft,

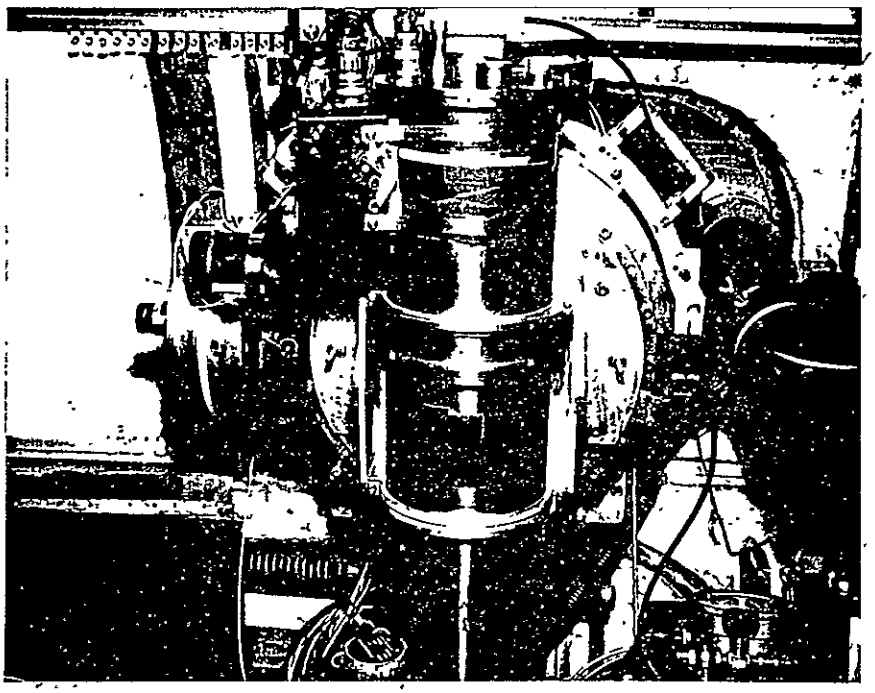

Figure 3-1. The Lear telescope seen from the back, with the spectrometer mounted. This photograph was taken during the March 1974 field trip.

and can be moved through 6 degrees of travel in the yaw and roll directions. By jacking the telescope up and down, sources which lie between 15 and 27 degrees off the horizon can be observed. The flight path is plotted by the navigator so that the source is at the right altitude off the horizon and the aircraft on the right heading when the observing period begins. Observations are generally made with the source as close to the upper limit of telescope travel as possible, in order to reduce the air mass. Typical flight duration is 2.5 hours, with from 40 minutes to an hour of observing time available on a source. More than one source can be observed on a flight, but the sources which can be observed on the same flight are restricted by the flight duration and the limited range of telescope travel.

The telescope is mounted in a bearing, and moves smoothly as long as the differential pressure between the inside and outside of the aircraft is less than about 5 lbs/sq.in. Hence the cabin pressure must be maintained at roughly 7 lbs/sq.in. during observations, which is equivalent to an altitude of more than 6 km. As a result, oxygen masks must be worn at all times during flight.

Observing Procedure

Data Acquisition System

The system employed during the March-April observing series is shown in block form in Figure 3-3. On previous

field trips, only one detector was used, but otherwise the signal processing was similar. A photograph of the electronics rack in the aircraft during the March 1974 field trip is shown in Figure 3-2.

On each flight two experimenters were aboard. One guided the telescope while the other ran the electronics, monitored the signal, and generally quarterbacked the operation.

Preflight Testing

Before each flight the instrument was run with a test source, to make certain that it was functioning properly. The ground spectra thus obtained were useful in data analysis as well, since any day-to-day changes in instrumental performance could be monitored. Such changes were small, and can probably be attributed more to changes in relative humidity in the hangar than to changes in instrument response.

Initial Flight Testing

The first couple of flights in each series were used for equipment testing as well as astronomical observations. The equipment was generally substantially modified between field trips, and performance in the air could not be completely predicted from ground tests. Also, a shakedown period always seemed to be necessary in order to become accustomed to working in the rather cramped quarters of the Lear Jet, while burdened with a flight helmet and an oxygen mask.

In the air, background flux on the detectors was much

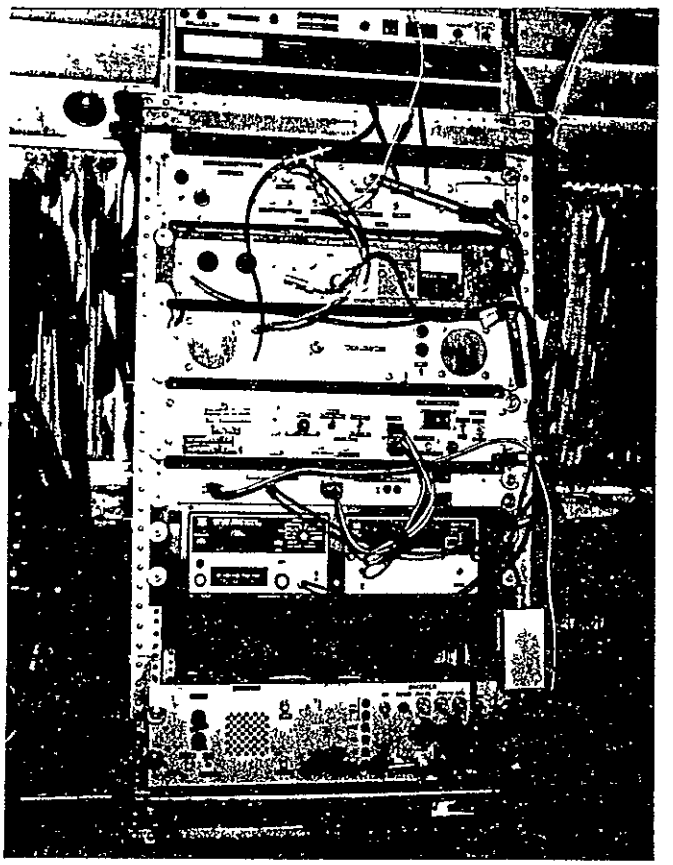

Figure 3-2. The electronics rack in the Lear Jet, from the March 1974 field trip. The equipment mounted is, from the top, the tape recorder, the VCO's, the lock-in amplifier, the audio amplifier, the stepping motor drive electronics, a junction panel, the counter and printer, and the chopping secondary electronics.

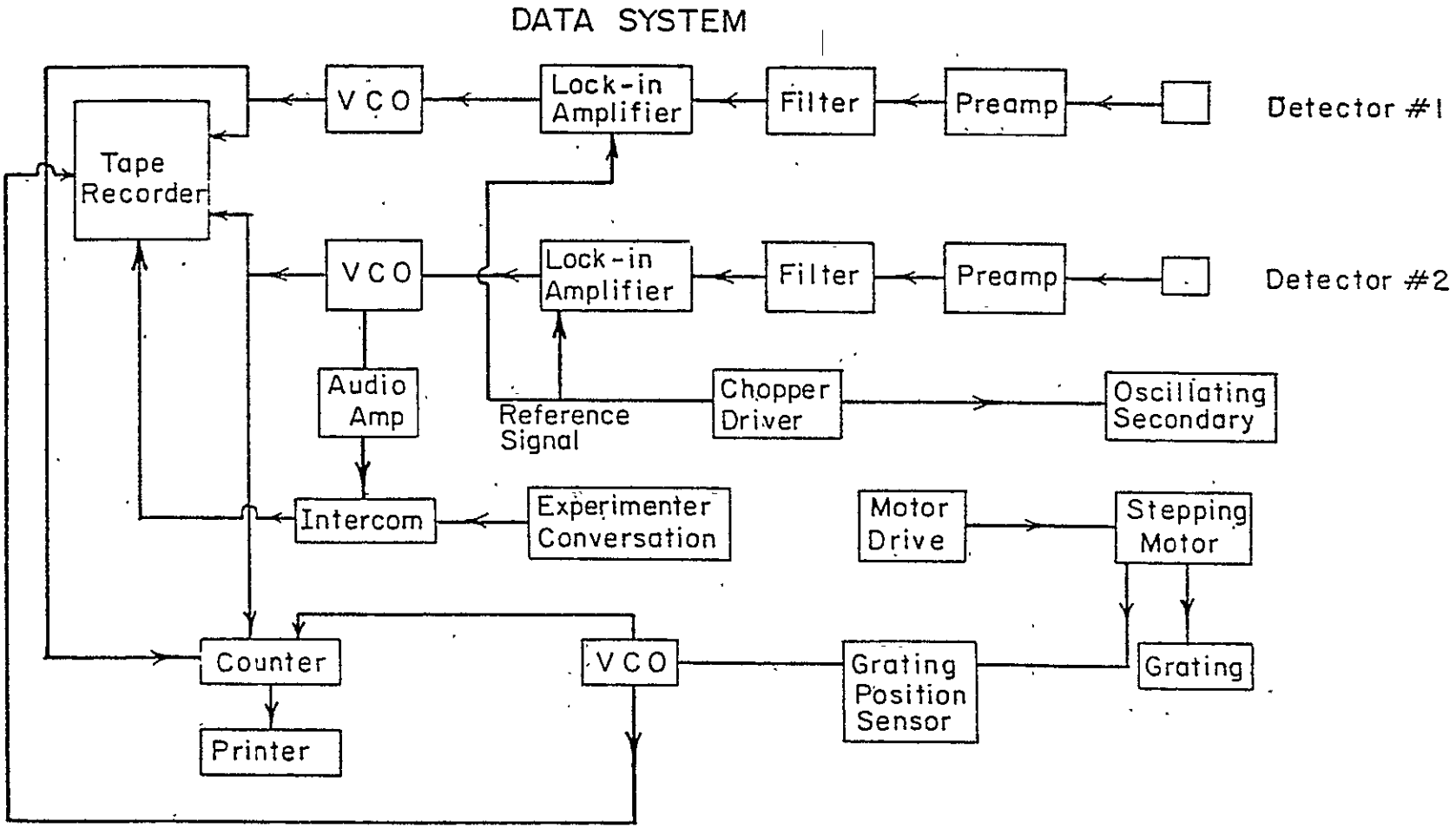

Figure 3-3. Schematic of the flight electronics. The arrows indicate the direction of the flow of information or control.

lower than on the ground, due to reduced emissivity and temperature of the atmosphere. This meant that the detectors became more sensitive, but usually also preferred somewhat different bias voltages than those which gave optimum signal to noise ratio during ground tests. Hence it was necessary to adjust bias once more to achieve reasonable noise levels. Once the best bias level had been determined, the bias remained unaltered throughout the rest of the observing series.

Extra noise due to microphonic pickup in preamplifier and detector leads was often a problem in early field trips, and progressive improvement usually occurred during the course of a field trip with the addition of filters and copious quantities of rubber sealant to stop vibration. The MOSFET preamplifiers seem to have eliminated this problem.

Since the telescope guiding was performed using a separate guide telescope, it was necessary at the start of each observing series to establish where the object should appear in the guide telescope in order to image on the spectrometer slit. This was done by first observing the moon to get a rough boresight, then moving on to Jupiter, Venus or M42, all of which are sufficiently bright to be easily detectable. The boresight thus established was used as first approximation for "peaking up" on the source during later flights, and remained relatively stable.

Procedure During Data Flights

Each data flight consisted of three phases--the climb

to altitude, the observing period, and the descent to land.

During the climb period all the equipment was normally turned on and checked out. From about 10 km on up to peak altitude, temperature and Mach number were recorded to give an indication if the aircraft had cleared the tropopause. The cabin was brought to 7 lbs/sq.in. pressure to free the telescope, so its movement could be tested. If everything was working well, time was also spent telling jokes and singing over the intercom to a captive audience.

Once peak altitude (usually about 13.7 km) was reached, there was often some dead time before we turned on course to observe the astronomical source. During this time more system checks were normally made, and often "offset spectra" were taken. These were spectra of the chopped emission from the telescope, which was normally nonzero, and often much larger than the astronomical signal. This emission was also found to be somewhat variable depending on the telescope orientation with respect to the aircraft. This gave an extra source of noise on some flights when the aircraft oscillated slightly in the roll direction due to turbulence.

When we turned on track, the observer would try to locate the source by identifying the field using the guide telescope, moved manually. Once he felt that he had located the source, he would turn on the gyros, and tell the pilot to "fly the needles." The "needles" were meters which indicated where the telescope was located with respect to its limits

of travel. The pilot would try to keep the telescope centered in the yaw direction by changing heading, and the observer would periodically jack the telescope up or down to stay centered in the roll direction.

On each flight, we "peaked up" on the source, with the observer trying to maximize the frequency of the signal fed back into the intercom from the voltage controlled oscillators (VCO's). On weak sources there was often sufficient noise so that this was a difficult process, and the other experimenter would monitor the signal level from the counter until it was maximized. Once the source signal had been maximized, the observer would guide on the same position for the rest of the flight, ignoring feedback from the signal over the intercom.

At this point, data recording would begin. During a flight we would go through the bandpass to be sampled by stepping the grating. Normally the steps taken corresponded to the resolution of the instrument, or somewhat smaller. Spectra were taken by stepping the grating one way as far as was desired, then going back to the start and repeating.

The procedure varied slightly, but always data on the source at one grating position would be followed by a period of observing on the sky. This was necessary to eliminate the offset signal previously mentioned. The "sky" observations were made 15 or 20 arc minutes away from the source, in the direction perpendicular to the chopper motion. We went directly from an "on" to an "off" at each grating

position to minimize the effects of drifts which were sometimes noticed. These drifts may have been due to the lock-in amplifiers, or perhaps due to the plane rolling slightly and changing the offset level.

Often more than one source was observed during a given flight, with the second source usually being the moon, so that an atmospheric calibration would be obtained on the same flight. During the last couple of flight series it has become evident that the atmospheric transmission is quite consistent as long as the aircraft is above the tropopause, so generally only one source has been observed per flight.

The pilots would inform us when the observing period was over, although sometimes if fuel reserves were adequate and the weather was good a few extra minutes of observation beyond the scheduled limits were possible. Once the observing time was finished, everything was turned off except the gyros, and popping one's ears (to avoid a painful ear block) became the major activity as the cabin pressure was brought back up. The telescope gyros were shut off only after the aircraft had come to a stop on the ground.

Data Analysis

The initial steps of the data analysis were the same for all of the observations, so I will discuss these steps in this section. The data analysis pertaining particularly to observations of a given object during a given field trip will be

discussed in connection with presentation of the results in later chapters.

Averaging and Normalization

The flight data were printed out in one-second integrations, and typically about ten values were taken "off" and then ten "on" at each grating position. The average value for each "off" and "on" was determined, and the difference taken to be the signal level. The standard deviation was also calculated to give a measure of the noise.

Thus for a flight in which we did n runs through m grating positions we had mn data points s_{ij}. However, systematic trends with air mass were noted, with values being typically lower for higher air mass. Hence a normalization was carried out, multiplying all the results from a given spectral run by a number k_j determined by the constraint that

$$k_j = \sum_{i=1}^{m} s_{ij} = K$$

where

$$K = \frac{1}{n} \sum_{i=1}^{m} \sum_{j=1}^{n} s_{ij}$$

This correction was generally relatively small, of the order of 10% over a flight.

Often data for a given object were taken on several nights, and systematic differences were noted between the

results. This seemed to be due to changes in how well the source was "peaked up" on a given flight. The result was a difference in overall signal levels, which was normalized out in the same manner as for data from one night. Again the differences were usually of the order of 10%.

A second systematic night-to-night change was a systematic shift in the effective wavelength for a given grating position. This occurred because many of the sources were smaller than our beam, and moving the image of the source in the entrance slit along the dispersion direction would change the effective wavelength of the light reaching the detector. Atmospheric transmission features were used to remove this effect. The spectra from different nights were moved relative to each other until the transmission features matched. Slight changes in the zero of the grating drive produced a similar effect, which was corrected by using transmission features in the ground tests to tell how much to shift the results.

Lunar Calibrations

The moon has been the main calibration source for all observations except those of the March-April 1975 field trip, where the calibration procedure will be discussed in Chapter V. It has been assumed that the moon radiates as a blackbody throughout our passband, with the temperature variation with phase angle given by Linsky (1973).

Observations of the moon were generally made with a

smaller step size over a wider bandpass than observations of other objects. This was possible because the signal levels were very high and it was not necessary to integrate very long to get excellent signal to noise ratios. The offset was much less than the signal level, so only "on" spectra were taken.

A moon spectrum from the March 1974 flight series is shown in Figure 3-4. This spectrum is typical of moon spectra at 4.5μ resolution. In general the moon spectra were very consistent throughout all the field trips as long as the aircraft cleared the tropopause.

A steady baseline appears on all the moon spectra. This baseline comes from scatter and lock-in zero offset, and was subtracted off before using the spectrum for calibration purposes, as is discussed in Chapter II. After this subtraction, the moon spectrum was divided by a blackbody spectrum of the appropriate temperature to get correction factors at each grating position for atmospheric transmission and instrumental profile.

This procedure was successful for all the early flight series, except for problems associated with the instrumental bandpass, as mentioned in Chapter II. However, installation of new filters and preamplifiers caused dynamic range problems to occur during the March-April 1975 field trip. In the future, calibrations will probably have to be made using planetary observations, with Mars being the most likely candidate since it has the fewest atmospheric complications.

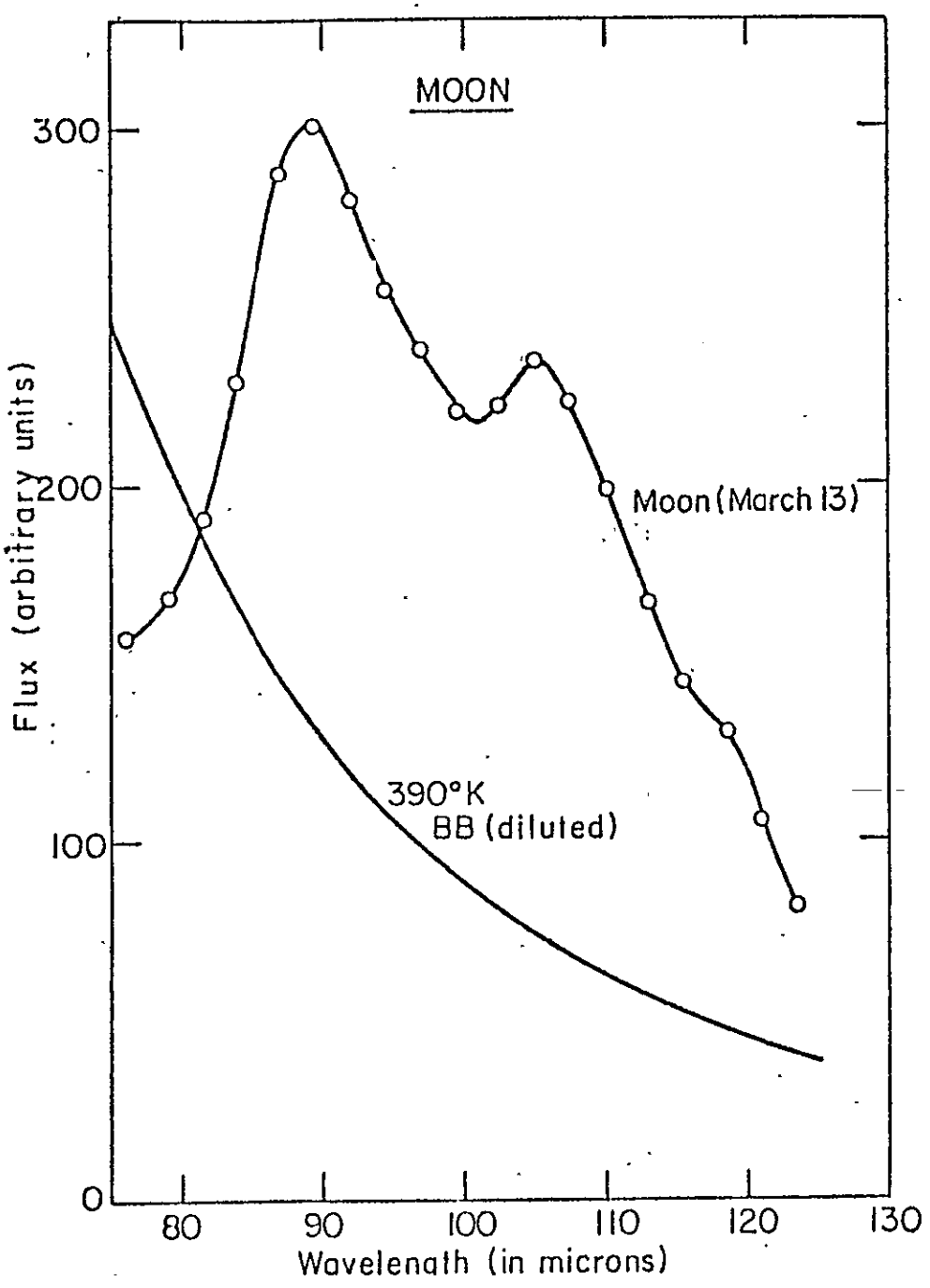

Figure 3-4. Typical raw moon spectrum from the March 1974 field trip, at 4.5μ resolution. A 390°K blackbody curve is also drawn to give an indication of instrumental sensitivity as a function of wavelength. Errors are too small to plot.

Error Analysis

The error bars given for the results in Chapters IV and V are derived from the variance of the mean of the individual observations, after normalization to correct for air mass changes and nightly variations, as described earlier in this chapter. It was found in all cases that the resulting error bars were larger than would be expected from the signal to noise ratio in a single observation at a given grating position. Also, chi-squared fits to the results often gave results at a very high confidence level, suggesting that the probable errors were substantially overestimated.

The conclusion reached is that some sort of systematic error is present which greatly increases the variance of the mean by causing a few bad points to be present. Guiding errors are one likely cause for this error. It has been noted that signal levels change dramatically for even a one arc minute change in pointing, so if the observer does not come back to exactly the same guiding position every time, fairly large errors could be introduced.

A second possible cause is changes in the atmospheric transmission during a flight. Water vapor measuring instruments on the C-141 which is also flown from NASA Ames often record sudden changes in the atmospheric opacity. However, this aircraft flies several thousand feet lower than the Lear, so these fluctuations may occur because the C-141 is flying near the tropopause.

If pointing error is the source of the problem, one solution may be to use a guiding eyepiece with a longer focal length, to expand the scale of the part of the sky being observed. This would permit the observer to point the telescope more accurately. Such an eyepiece is now available, and will be tried in the future.

CHAPTER IV

HIGH RESOLUTION OBSERVATIONS OF H II REGIONS

The high resolution spectroscopy carried out from the Lear Jet was almost completely devoted to a search for the (O III) 88.16μ fine structure line. In the first section of this chapter a brief discussion of the O III line and other fine structure lines will be given. The next two sections will present the results of observations of the Orion Nebula (M42) and the Omega Nebula (M17). The last section of the chapter will compare observational results to theoretical predictions, and discuss the applications of infrared fine structure lines in determining the characteristics of H II regions.

Infrared Fine Structure Lines

Fine structure lines from ions are produced by transitions between the fine structure levels of the ion. The levels for various configurations of electrons are shown in Figure 4-1 taken from Simpson (1975). The lines are typically in the infrared region of the spectrum, and examples are given in Table 4-2 which is also taken from Simpson. Lines from the ground states of the ions are most important, since for an ion in an excited state the transition probability to emit an optical or ultraviolet photon is much higher than the

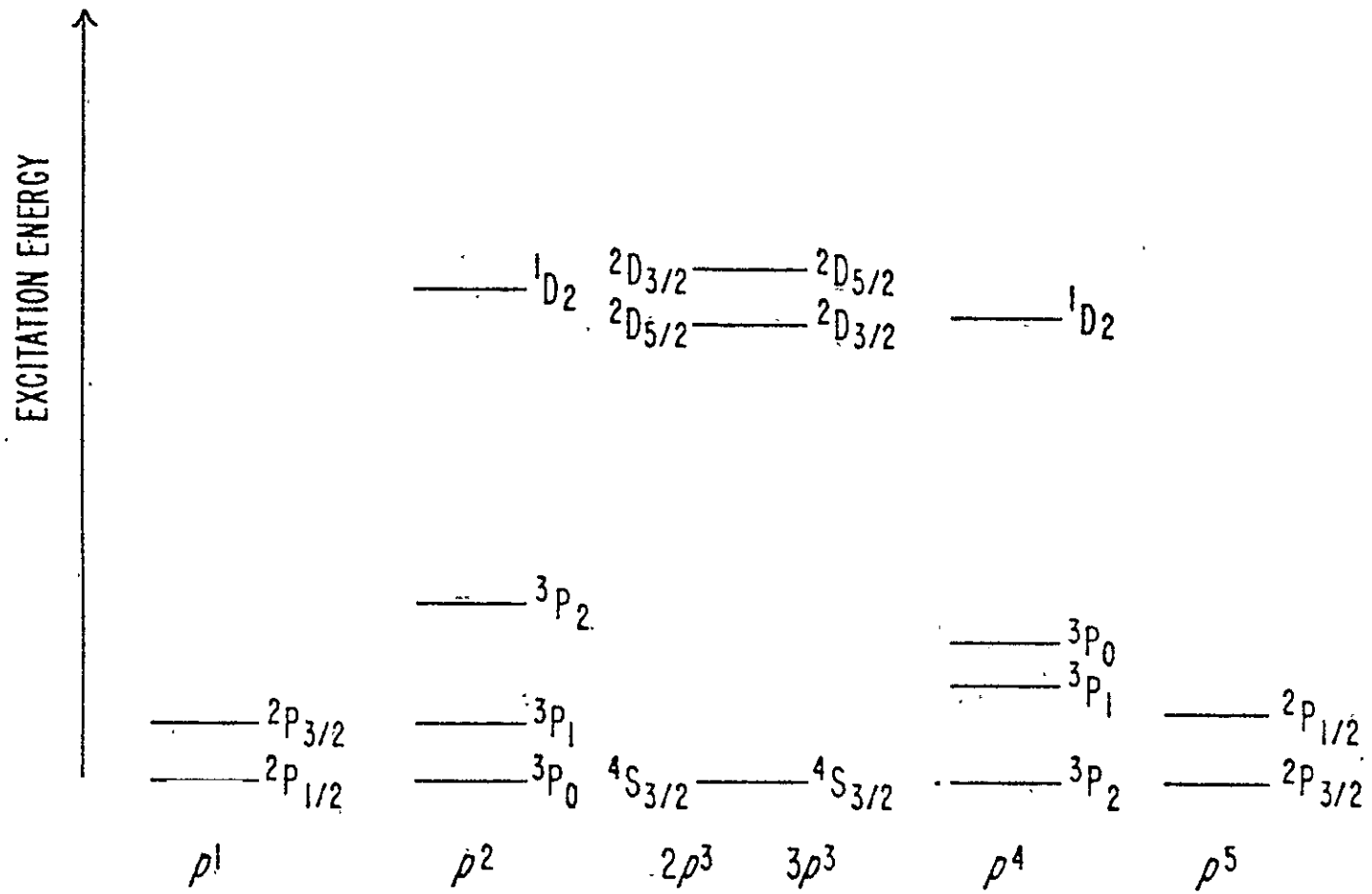

Figure 4-1. The lower energy levels for electron configurations from p^1 to p^5, taken from Simpson (1975).

probability to undergo a fine structure transition. For this reason ions of the p^3 configuration which have no ground state splitting will emit only exceedingly weak fine structure lines.

Ions of the p^2 or p^4 configurations have three ground state fine structure levels. There are thus three possible transitions, but $1 \rightarrow 0$ and $2 \rightarrow 1$ can go by means of magnetic dipole interactions, and are much faster than $2 \rightarrow 0$ which is an electric quadrupole transition. (The direction of the arrows is for the p^2 configuration--the p^4 configuration has the arrows going the opposite way.) The p^1 and p^5 configurations have two ground state fine structure levels and give rise to only one line, again by a magnetic dipole transition.

In H II regions the most important mode of excitation for these lines is by collision with electrons. According to Petrosian (1970), for the typical electron density of 10^3 cm^{-3} and electron temperature of 10^4°K of an H II region, the collisional excitation probability is roughly 10^{-4} sec^{-1}. Petrosian goes on to point out that in order to reach this excitation probability level, excitation by protons requires far higher temperatures, and that direct photon excitation or excitation by cascade after absorption of an ultraviolet photon both require far higher densities of radiation than are normally found in H II regions.

O III is an example of an ion with a p^2 configuration, and has lines at 88.16μ and 51.69μ. These wavelengths must be determined from optical measurements, since the lines

have not been detected in the laboratory. The line positions derived from these optical measurement are accurate to about ± 0.1μ. The natural width of the line is exceedingly narrow because of the small transition probability (2.5×10^{-5} sec^{-1} for (O III) 88.16μ). Even after considering the effect of motions within the nebulae, the line width is far narrower than the 1.3μ bandpass of the spectrometer.

Observations of M42

The observations of M42 were carried out from the Lear Jet in November 1974, using a beam roughly 5 arc minutes square and a bandpass of 1.3μ full width at half maximum. The procedure followed during observations was as described in Chapter III. The results of three flights are plotted in Figure 4-2, after calibration with moon spectra to remove instrumental profile and atmospheric transmission features. Each point represents the average of data from one flight for a given grating position, but because of instrumental changes between flights, measurements were taken at slightly different wavelength settings on successive flights. The points have been normalized to correct for air mass effects and daily variations in sensitivity. The error bars are one standard deviation, the major source of error being guiding noise.

The line drawn on Figure 4-2 is a 75°K blackbody function diluted to fit all points except those around the O III

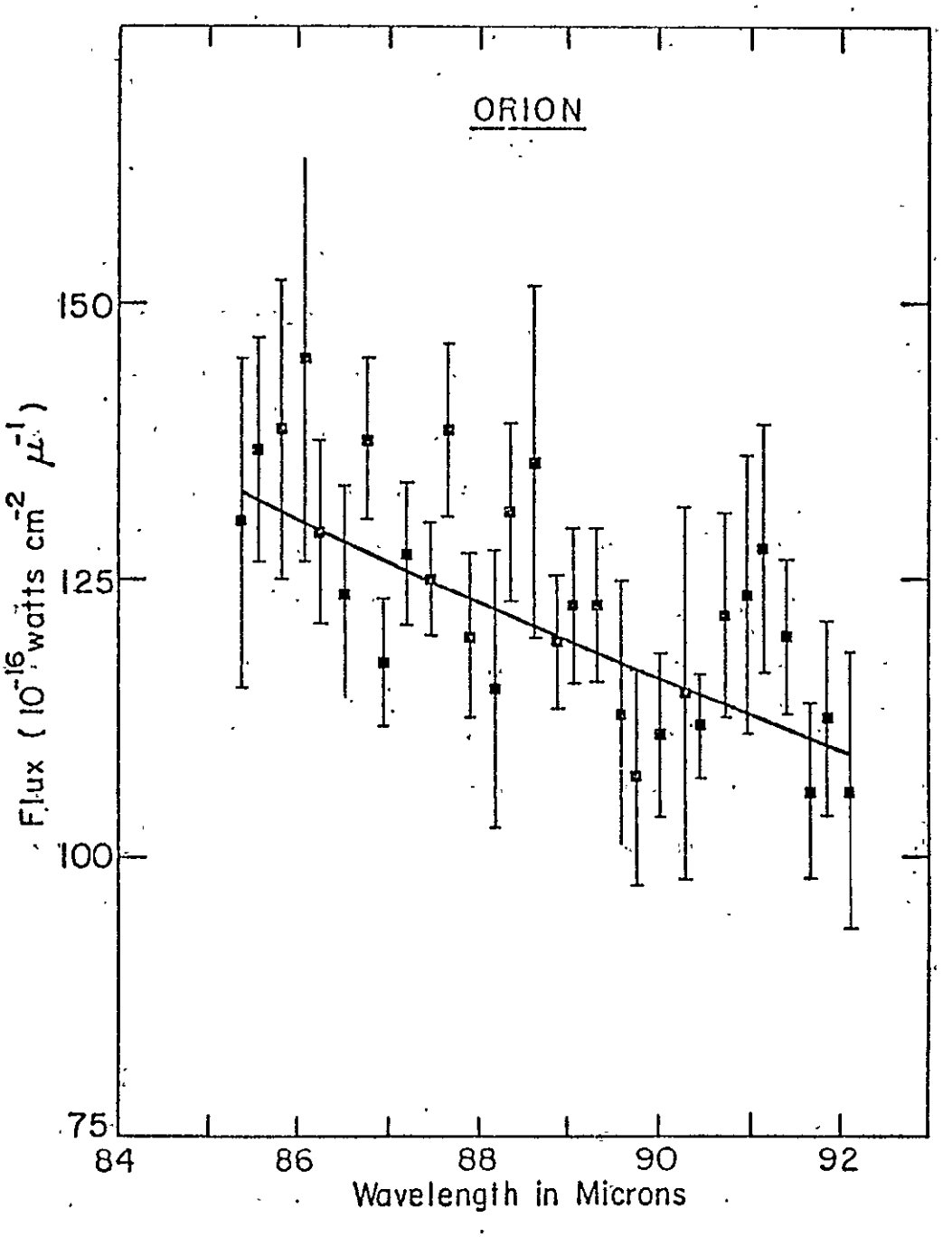

Figure 4-2. Spectrum of the Orion Nebula (M42) at 1.3μ resolution, after calibration with lunar spectra. Error bars are one standard deviation. The line is a 75°K blackbody function diluted to fit the data.

line position. The temperature used for the fit was not critical, and a straight line fit looked very similar over this short range of wavelengths. The absolute flux level is taken from Harper (1974), who also used a 5 arc minute beam.

The only obvious features in the spectrum are the bump at 91μ and the dip at 90μ due to atmospheric transmission variations which have not been completely removed by lunar calibrations. However, the atmospheric transmission spectrum is quite smooth around 88μ, and no major calibration problems should exist there. The wavelength of the O III line is known to within ± 0.1μ from observations of optical lines, and the wavelength scale is in error by at most ± 0.3μ. Hence, in the absence of any feature around 88μ, we must conclude that it is not possible to detect the (O III) 88.16μ line in Orion at our resolution and sensitivity.

In order to establish an upper limit on the flux in the line the instrumental response to a narrow line was approximated by a sawtooth function of a half width corresponding to the resolution of the spectrometer. This was run through the spectrum between 87μ and 89μ, and no significant maximum appeared. At three standard deviations, the upper limit is $2 \pm 0.5 \times 10^{-15}$ watts cm^{-2} for the line intensity. The error limits are derived from the errors given by Harper (1974) for the absolute flux levels.

Observations of M17

M17 was observed in April 1975 using a beam of roughly 4 x 5 arc minutes and a bandpass of 1.3μ. Again the observing procedure was as described in Chapter III. Observations were made of Venus and the moon during the same flight series. The results for these three sources are plotted in Figure 4-3, along with the M42 results discussed in the previous section.

The spectra shown in Figure 4-3 are not corrected for atmospheric transmission or instrumental profile. However, in order to make direct comparison simpler, the raw spectra have been divided by black body functions of appropriate temperatures to remove the overall slopes. Also, the spectra have been normalized to the same scale. The blackbody temperatures used were 390°K for the moon (Linsky, 1973), 245°K for Venus (Chase et al., 1974), 75°K for M42 from coarse resolution data given in the next chapter, and 80°K for M17 from Harper (1974). Over this short range of wavelengths errors in the temperatures are not critical.

A number of spectra were taken during observations of each object, and these were normalized to remove small air mass effects, then averaged to obtain the spectra shown. The error bars are one standard deviation, derived from the variance of the mean of the data points at each grating position. The major noise component was guiding noise.

The M17 spectrum shows a strong feature at 88.1μ, more

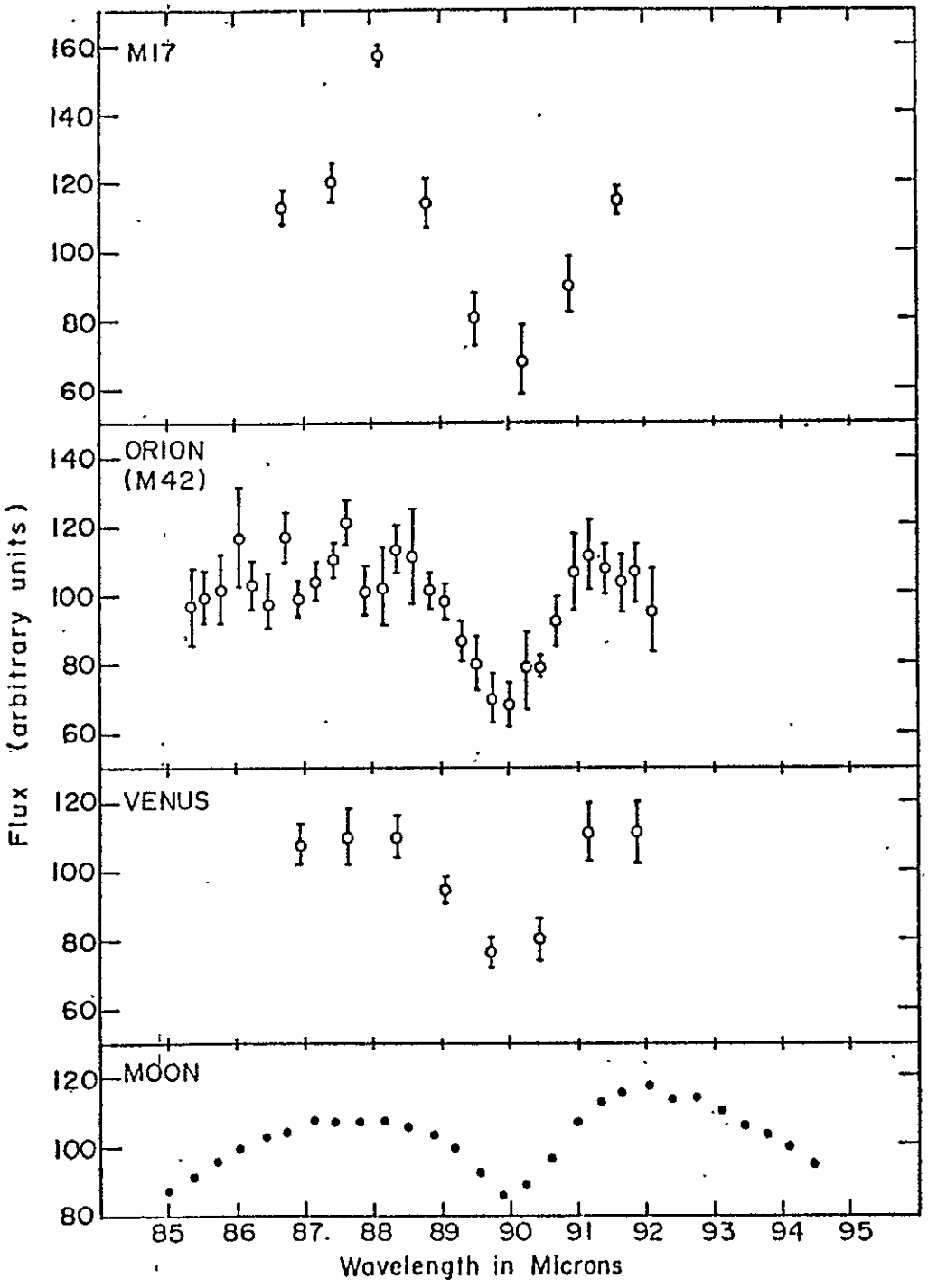

Figure 4-3. Spectra of M17, M42, Venus and the moon at 1.3μ resolution. The spectra have not been corrected for instrumental or atmospheric effects, but have been divided by blackbody functions of appropriate temperatures to remove overall slopes, and normalized to the same scale.

than 8 sigma above the neighboring points. This feature appeared in all seven individual spectra. The atmospheric transmission at this wavelength is quite smooth, as can be seen from the other spectra plotted. We suggest that this feature is the (O III) 88.16μ line.

The strong absorption feature seen at 90μ is due to atmospheric water vapor. This feature is broader and shallower in the lunar spectrum because the spectrometer has a slightly wider bandpass for sources like the moon which uniformly fill the entrance slit.

During the observations of M17 we guided on a position which gave the maximum continuum flux. To obtain the line intensity I_L for this region, one can use

$$I_L = \frac{S_L}{S_C} F_C \Delta\lambda$$

where S_L is the line signal, S_C is the continuum signal, $\Delta\lambda$ is the spectrometer bandpass and F_C is the continuum flux per unit wavelength interval. Using a continuum flux of 4.6 x 10^{-15} watts $cm^{-2}\mu^{-1}$ derived from the results of Harper (1974), who used a beam of roughly the same width as ours, we get a line intensity of $2.2^{+1.0}_{-0.7}$ x 10^{-15} watts cm^{-2}.

A major part of the uncertainty in the calculated value is due to the possible error in F_C, which can be as much as 25% according to Harper (1974). Other important sources of uncertainty are possible errors in the wavelength calibration,

the line and continuum signal levels, and the bandpass.

Comparison to Theoretical Predictions

The results obtained for the (O III) 88.16μ line can be compared to theoretical predictions by Petrosian (1970) and Simpson (1975). Both authors have made predictions for the intensity of a number of infrared fine structure lines in M42.

In order to predict line intensities, Petrosian develops a formula relating the intensity of a given fine structure line to the thermal radio flux density at a frequency ν_R (where $\tau_R << 1$). This relation is

$$\frac{I_i}{K_i \gamma_i} = \left(\frac{10^4 {}^\circ K}{T_e}\right)^{0.15} \left(\frac{\nu_R}{10^9 \text{ Hz}}\right)^{0.1} S(\nu_R) \ 3.7\times10^{-9} \ \text{erg/cm}^2\text{-sec.}$$

where I_i is the intensity of the fine structure line, $\gamma_i \times 10^{-4}$ is the abundance of the ion relative to the abundance of hydrogen, T_e is the electron temperature and $S(\nu_R)$ is the radio flux in flux units from the H II region. For p^1 and p^5 configurations,

$$K_i = \left(\frac{\Omega_{21}}{\omega_1}\right)_i \times \left(\frac{10\mu}{\lambda_i}\right)$$

where Ω_{21} is the collision strength for the ion, ω_1 is the statistical weight of the lower state, and λ_i is the wavelength of the line. The temperature dependence of the collisional excitation probabilities through the Boltzmann factor

has been ignored, since it is small for $\lambda > 10\mu$.

Petrosian defines a parameter x, given by

$$x = \left(\frac{n_e}{10^3 \text{ cm}^{-3}}\right)\left(\frac{10^4 ^\circ K}{T_e}\right)^{1/2}$$

where n_e is the electron density. He also defines a critical value x_{crit} for this parameter

$$x_{crit} = 69.6 \left(\frac{10\mu}{\lambda}\right)^3 \frac{\omega_1}{\Omega_{21}}$$

which determines when the fine structure levels become saturated. The formula for K_i is accurate in the low density limit, where de-excitation by radiation dominates de-excitation by collision. In the high density limit, $x >> x_{crit}$, the relation for K_i must be multiplied by x_{crit}/x, as collisional de-excitation dominates.

For ions like O III with p^2 or p^4 configurations

$$K_i(21) = \left(\frac{\Omega_{02}}{\omega_0}\right)_i \left(\frac{10\mu}{\lambda_{21}}\right)_i$$

$$K_i(10) = K_i(21)\ R_{fs}$$

where R_{fs} is the ratio of the intensities of the two fine structure lines, and is obtainable from the general expressions for a three level system (e.g. Aller and Liller, 1968). Petrosian obtains values of Ω_{ij} from published theoretical

calculations, and the values for ω_i are determined for each ion from $\omega_i = 2J_i + 1$. The wavelengths for the various lines are derived from optical measurements. The remaining parameters are derived from observations. Values for γ_i for various ions are obtained from optical forbidden line observations. The values for T_e, n_e and $S(\nu_R)$ are taken from radio continuum and recombination line observations, in which spherical constant density models are assumed.

Simpson (1975) derives emissivity values for various ions as a function of electron temperature and density, using values for Ω_{ij} from the literature and including the Boltzmann temperature dependence of the collisional excitation probability. An example of her results is plotted in Figure 4-5. She then uses these emissivity values to derive line intensities from a model (Simpson, 1973) for the Orion Nebula.

This model was designed to agree with the optical and radio observations of the nebula. Her model is also spherical, but has variations of electron temperature and density, with both peaking strongly toward the center of the nebula. She uses electron temperatures, densities and ionic abundances derived from forbidden line observations. In order to match these to the radio continuum observations, her spherical model must have the O II (whose optical forbidden lines give a measure of the density) be in clumps surrounded by a more tenuous medium.

The predicted intensities for M42 are presented in

Table 4-1, along with the observed upper limit. Simpson's result has been scaled to the spectrometer beam size. In addition, approximate intensities are given for M17, derived by using the M42 predictions following a procedure given by Petrosian (1970). These estimates have also been scaled to our beam size.

The predictions obtained from the results of Petrosian are substantially higher than the observed intensities for both M17 and M42, while those of Simpson seem to agree fairly well, although there are large uncertainties. Simpson's values are lower than those of Petrosian because of the lower O III abundance she assumes, and the higher central density of her M42 model, which reduces (O III) 88.16μ emission through collisional de-excitation.

Applications of Infrared Line Measurements

The (O III) 88.16μ Line

One obvious application of the (O III) 88.16μ line measurements has been illustrated in the previous paragraph. H II region models can be tested by calculating the amount of line emission they predict, and then checking to see if this matches observations. However, the result of such a comparison may not be particularly useful, since the (O III) 88.16μ line intensity depends strongly on the ionic abundance and the electron density and more weakly on electron temperature. If disagreement exists between predicted and observed

Table 4-1. Predicted and Observed Intensities for (O III) 88.16μ.

	Predictions		Observations
Source	Intensity (watts cm^{-2})	Reference	Intensity* (watts cm^{-2})
M42	3.9×10^{-15}	Petrosian (1970)	$<2^{+0.5}_{-0.5} \times 10^{-15}$
	1.4×10^{-15}	Simpson (1975)	
M17	$\sim 6 \times 10^{-15}$	Petrosian (1970)	$2.2^{+1.0}_{-0.7} \times 10^{-15}$
	$\sim 2 \times 10^{-15}$	Simpson (1975)	

*The line intensity is more easily measured in M17 because the continuum is weaker.

intensities, it may be difficult to assess which parameters of the H II region model must be altered.

It would be much more satisfactory to be able to isolate one parameter, and use the line information to give a value for this parameter. A way to do this is to take a ratio between the 88μ line intensity and the intensity of some other line from O III. The result will not depend on the abundance of the O III ion. Bergeron (1975) suggests that the ratio of the 88μ line and the (O III) 5007Å line intensities be employed in this fashion. The ratio that results is

$$\frac{I(88\mu)}{I(5007\text{Å})} = \frac{j(88\mu)}{j(5007\text{Å})} C_{H\beta} \left(\frac{A_{IR}}{A_{OPT}}\right)$$

Here $j(88\mu)$ and $j(5007\text{Å})$ are emissivities for the 88μ and 5007Å lines respectively, and $C_{H\beta}$ is a reddening correction for the 5007Å line. The last term is the ratio of the angular areas observed in the infrared and optical measurements.

The emissivity of (O III) 5007Å $\sim n_e^2 f(T_e)$, but T_e is determined fairly accurately by the ratio of O LII optical forbidden lines. The emissivity of the 88μ line is $j(88\mu) \sim n_e^2$ for low densities, but for n_e greater than 10^3, $j(88\mu) \sim n_e$ because collisional de-excitation competes with radiative de-excitation to depopulate the upper states. The variation of emissivity with density is shown in Figure 4-4 taken from Simpson (1975).

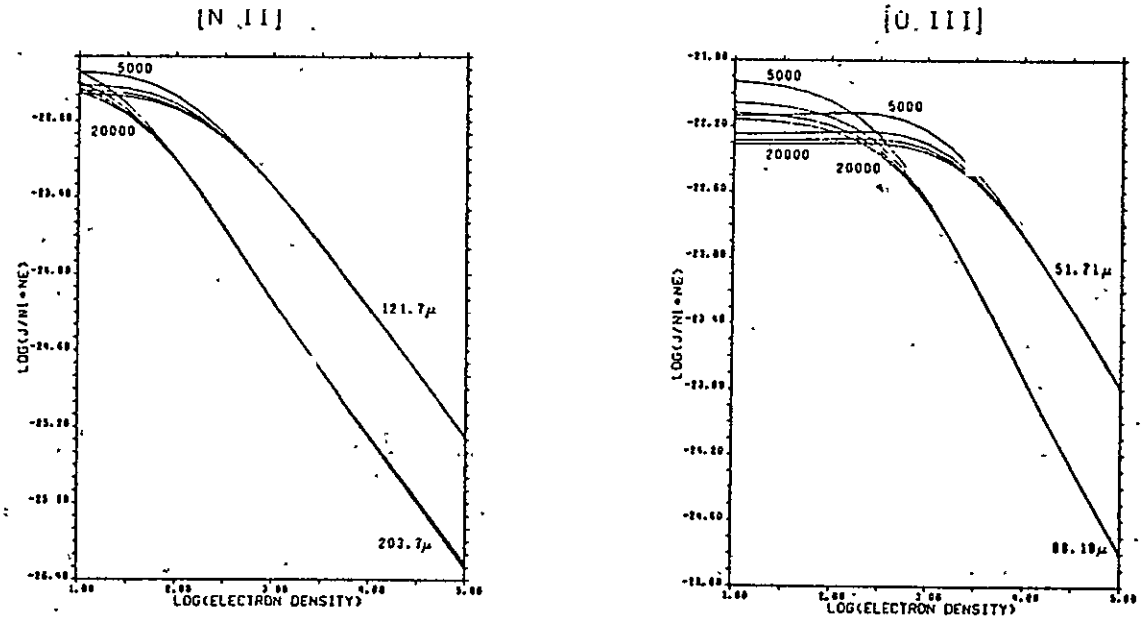

Figure 4-4. Log(j/N_iN_e) for O III and N II fine structure lines as a function of electron density and temperature, where j is the emissivity and N_e and N_i are the electron and ion number densities. This figure was taken from Simpson (1975).

Thus, for number densities greater than 10^3,

$$\frac{j(88\mu)}{j(5007\text{Å})} \propto n_e^{-1}$$

and the observed ratio can be used to determine the electron density as long as the reddening correction and the ratio of the regions sampled in the infrared and optical are known accurately.

In actual practice, there are liable to be complications when one attempts to apply this method to learn the electron density of a region. Infrared beam sizes are often hard to measure accurately, and are in any case much larger than typical beam sizes for optical observations. Hence scaling the optical data to the infrared beam size may lead to large uncertainties, particularly if the surface brightness of the region in (O III) 5007Å is not uniform. Also, in many cases infrared beam sizes are of the order of the size of the H II region, at least for Lear Jet observations, and one can only determine average electron densities for a whole source by this method. It would be more interesting to be able to use higher angular resolution and get electron density distributions across the source. Another problem occurs if the source contains a lot of dust. In this case, the reddening correction will be difficult to determine, and the ratio of the 88μ and 5007Å intensities will be observed to be higher than the

actual density would yield, because much of the 5007Å emission will have been absorbed inside the object.

However, despite these drawbacks, this method can be applied usefully to some sources. For the Orion Nebula, observations of (O II) 3726/3729 Å indicate high electron densities (Osterbrock and Flather, 1959; Simpson, 1973), high enough that homogeneous spherical models would yield far too much radio flux. Hence any spherical model must have high density clumps containing the O II surrounded by a more tenuous medium (Simpson, 1973) in order to explain the observations. This type of model is supported by the fact that O II and O III forbidden lines give different temperatures, and one might postulate a region with dense clumps containing the O II and a more tenuous medium containing mostly O III. Applying the method outlined above to determine the electron density in the O III line emitting region, Bergeron (1975) finds that the observed upper limit on the (O III) 88.16μ line emission means that, in a spherical model, a major part of the (O III) 5007Å emission must also come from dense clumps, which have to contain an important fraction of the mass of the nebula. Zuckerman (1973) has suggested that the Orion Nebula may be a relatively thin, dense sheet across the front of the Orion molecular cloud. This model agrees with the results obtained using the 88μ line, and is supported by recent maps of the Orion region in the far infrared (Werner et al., 1975).

Future Applications of Infrared Lines

The detection of the (O III) 88.16μ line is only the first step in utilization of the far infrared fine structure lines as an astrophysical tool. There are a number of other lines which should be detectable with present sensitivity from above the atmosphere. The strongest lines in the near and far infrared and their expected intensities in M42 are shown in Table 4-2, which is taken from Simpson (1975). Two major applications of observations of these lines would be in the determination of electron density and ionic density.

The electron density would be best measured using the ratio of the intensities of different lines from the same ion. Referring again to Figure 4-4 from Simpson (1975), it can be seen that the ratio of intensities of (O III) 88.16μ and (O III) 51.69μ is a sensitive measure of the electron density for densities between 10^2 and $10^3 cm^{-3}$. Furthermore, this ratio is relatively insensitive to the temperature, as can be seen from the results given for temperatures between 5000°K and 20,000°K in the same figure. Both lines are quite strong--indeed, the 51.69μ line is expected to be stronger than the 88.16μ line in M42. Other pairs of infrared lines would be useful at higher and lower densities, as has been shown by the results of Simpson (1975).

This approach would be particularly useful in regions where visible obscuration precludes the measurement of electron density with the optical forbidden lines of O II or S II.

Table 4-2. Predicted Line Strengths for the Orion Nebula--Simpson (1975).

Line	Wavelength (microns)	Flux (ergs $cm^{-2}sec^{-1}$)
(Ar II)	6.98	2.00×10^{-9}
(Na III)	7.33	7.00×10^{-10}
(Ar III)	8.99	3.65×10^{-9}
(S IV)	10.52	1.39×10^{-7}
(Cl IV)	11.76	3.03×10^{-10}
(Ne II)	12.79	2.92×10^{-8}
(Cl II)	14.35	2.21×10^{-10}
(Ne III)	15.38	3.16×10^{-8}
(P III)	17.9	6.20×10^{-10}
(S III)	18.68	1.19×10^{-7}
(Cl IV)	20.37	4.06×10^{-10}
(Ar III)	21.4	2.62×10^{-10}
(Cl II)	33.4	1.62×10^{-11}
(S III)	33.65	1.12×10^{-7}
(Si II)	34.8	9.39×10^{-9}
(Ne III)	36.10	2.35×10^{-9}
(O III)	51.71	5.84×10^{-8}
(N III)	57.31	8.73×10^{-9}
(O III)	88.18	2.71×10^{-8}
(N II)	121.7	2.56×10^{-9}
(C II)	156.3	6.70×10^{-10}
(N II)	203.7	8.17×10^{-10}

Obscuration problems make the near and far infrared fine structure lines perhaps the only source of information concerning elemental abundances and ionization structure in many regions, examples being the radio sources like W51, W49 or Sgr A which have no visible counterpart. In addition there are many ions with electron configurations p^1 or p^5 which do not have optical forbidden lines and whose recombination lines are usually too weak to be observed. For these ions, the infrared fine structure lines may again be the only means of determining abundances. Intensities of some of the lines from p^1 or p^5 configurations can be measured from the ground through atmospheric transmission windows, but the majority can only be observed from airborne platforms.

Unfortunately, many of the more interesting fine structure lines in the far infrared are blocked at airplane altitudes by atmospheric water features. An example is (O III) 51.69μ which is very close to a strong atmospheric water line. Full exploitation of the potential of the far infrared lines will come only with balloon or satellite observations. With these observing platforms lack of atmospheric absorption, low background fluxes and long integration times should permit the detection of far infrared lines in a wide variety of objects.

CHAPTER V

COARSE RESOLUTION OBSERVATIONS OF H II REGIONS

In this chapter data obtained during coarse resolution observations of M42 and M17 will be presented. The first section will be devoted to the M42 data, with subsections describing the results obtained during each of the last three field trips. The second section will describe the M17 results, and the last part of the chapter will discuss the results and indicate possible future observations.

M42 Observations

The March 1974 Field Trip

Observations during this flight series were carried out at roughly 4.5μ resolution with a beam 5 arc minutes square. The results are shown in Figure 5-1 after division by the moon spectrum to correct for instrumental profile and atmospheric transmission features. The absolute flux calibration is based on a temperature for Venus (289 ± 20°K) from Armstrong et al. (1973), and utilizes Venus observations made during the same week.

Superposed on the Orion data are 60 and 100°K blackbody curves diluted to give the right intensity. Better fits can be obtained by using grain emissivities of the form λ^{-n},

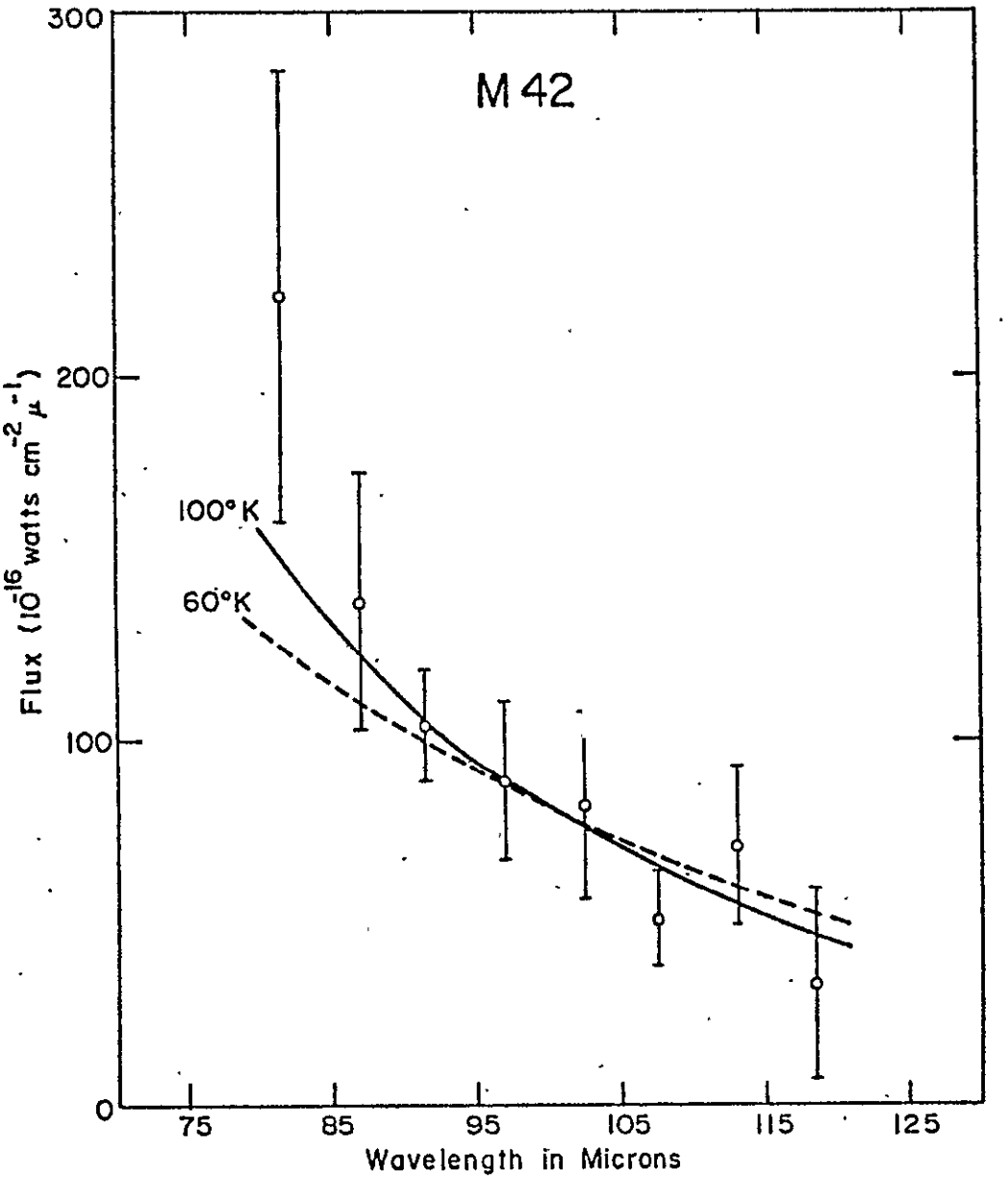

Figure 5-1. Spectrum of M42 from March 1974 field trip, calibrated with lunar spectra. The error bars are one standard deviation, and the 60°K and 100°K blackbody curves are diluted to fit the data.

but the difference is not statistically significant, in view of the rather low signal to noise ratio of the data.

The November 1974 Field Trip

Observations were made with the same bandpass and beam as in March, but considerably better sensitivity made detection of Orion relatively simple, and signal to noise ratios became much better. The results are plotted in Figure 5-2, again after division by lunar spectra. The absolute flux calibration is derived from the results of Harper (1974), who used a beam of similar width to ours.

The results have been fitted with blackbody curves at 50, 75 and 100°K. The best fit is at 75°K, and temperatures below 60°K do not fit well. Higher temperatures fit the curve reasonably well, as may be seen for the 100° curve plotted.

Some systematic error is possible, since a relatively large scatter correction had to be made for these observations. The central black spot fell off the secondary mirror of the spectrometer, and light could bounce back directly from the entrance slit into the detector. This effect could raise the end points of the curve by perhaps 5%. This would not greatly alter the results of the fit.

The March-April 1975 Field Trip

Coarse resolution observations were carried out at 5μ (second order) and 10μ (first order) resolution during this flight series, and the total available bandpass was expanded

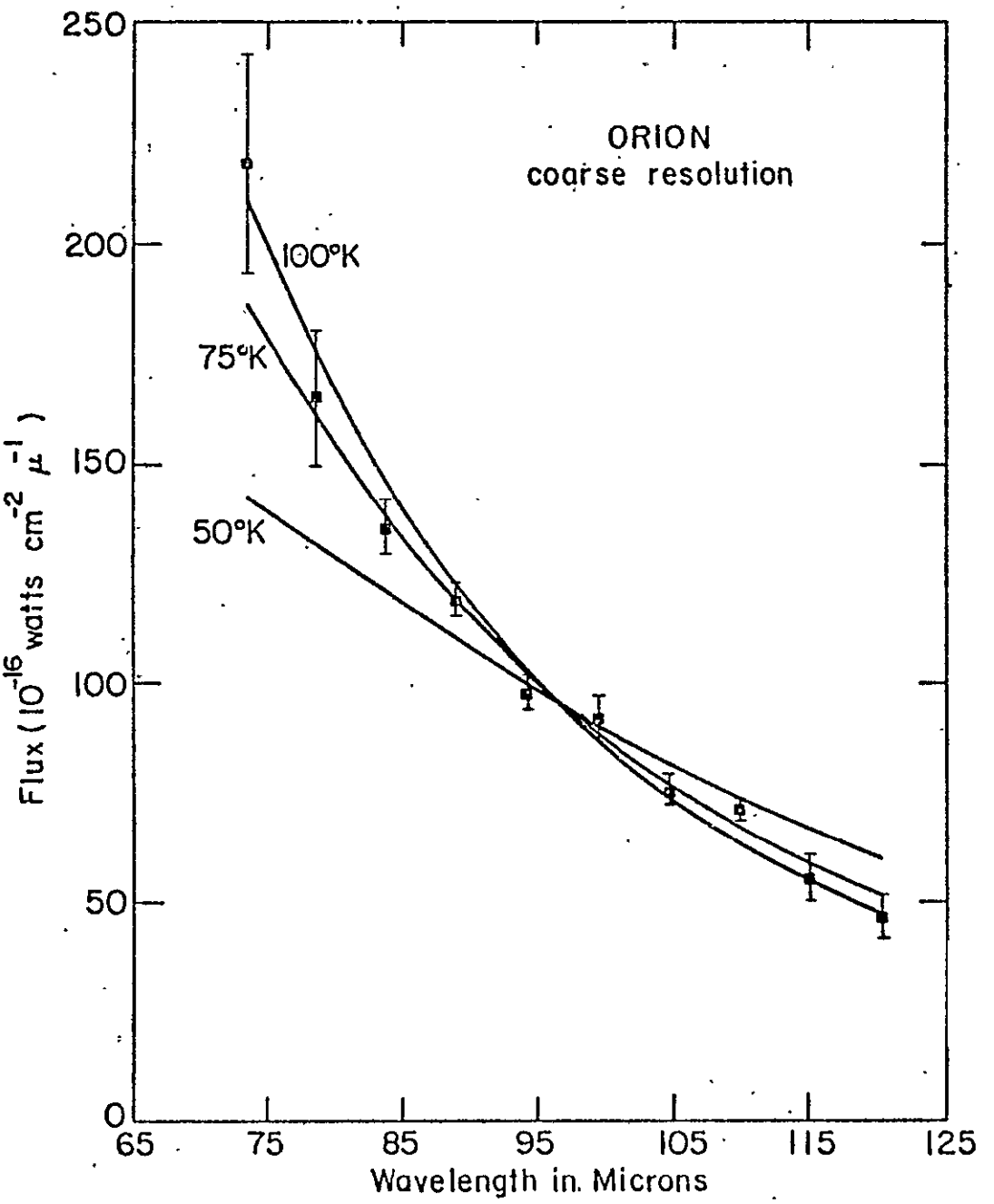

Figure 5-2. Spectrum of M42 from the November 1974 field trip, calibrated with lunar spectra. Error bars are one standard deviation, and the 50°K, 75°K and 100°K blackbody curves are diluted to fit the data.

to the range between 45μ and 115μ. The beam size was roughly 4 x 5 arc minutes. Considerably better sensitivity was achieved using new filters and a MOSFET preamplifier, but at the cost of severe nonlinearity of response for different background levels, as described in Chapter II. As a result, lunar calibrations were very inaccurate, and the results shown in Figure 5-3 were calibrated using the offset signal from the telescope. Figure 5-3 also shows the data from the November 1974 field trip and Harper's broadband observations of M42 and M17.

The line drawn on the figure corresponds to a diluted 105°K blackbody fit to the March-April 1975 data. The error bars are one standard deviation, and the absolute flux levels are again derived form the results of Harper (1974) at 91μ.

M17 Observations--The March-April 1975 Field Trip

The M17 observations were done with the same resolution and beam as the Orion observations on the same field trip. The results are also plotted in Figure 5-3. The error bars are one sigma, and the flux calibration is from the 93μ point of Harper (1974). The data plotted were obtained on one flight.

The M17 results show a strong far infrared excess. This excess showed up in the data from three flights, and its reality seems very probable. The data from the other

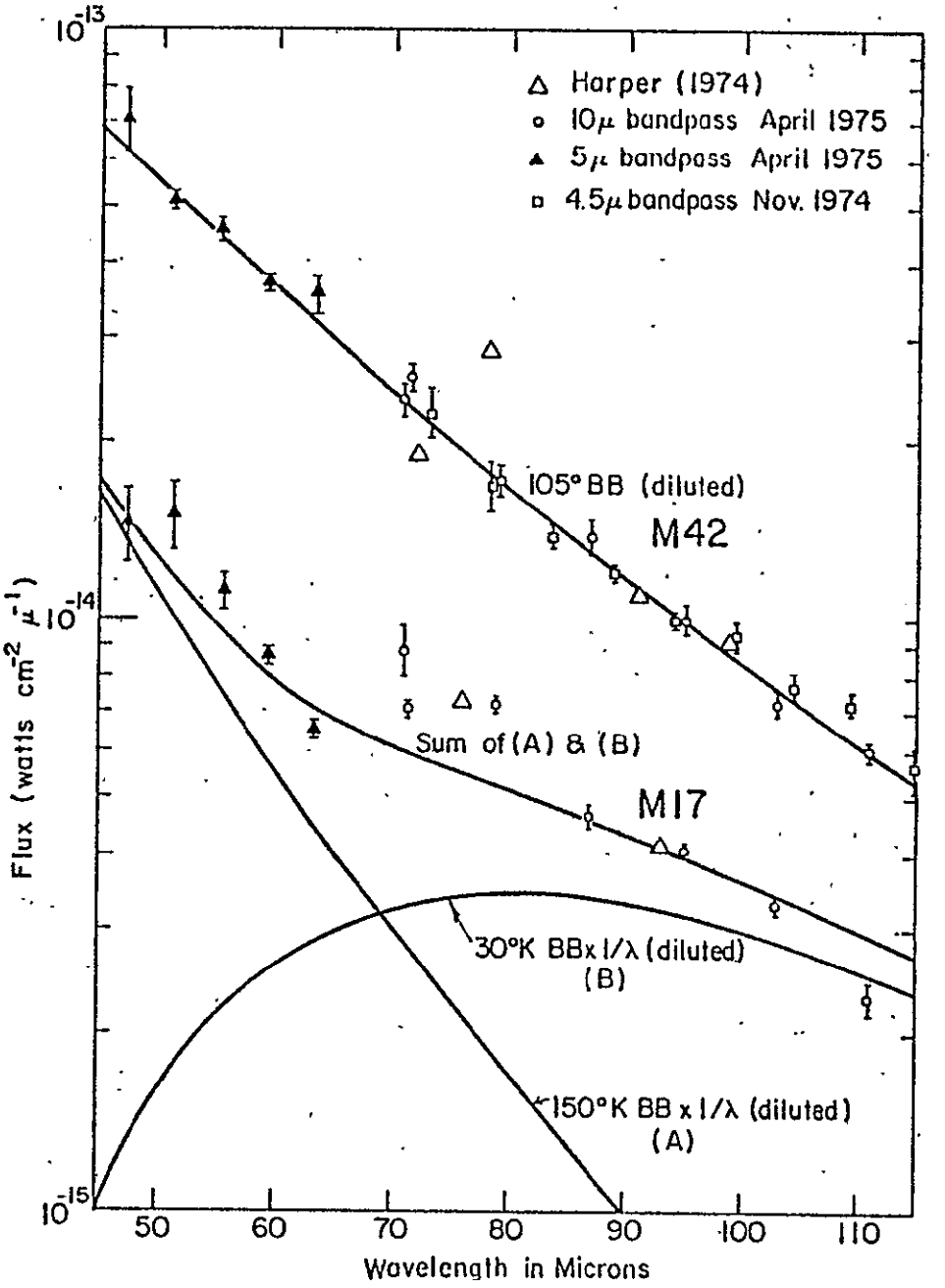

Figure 5-3. Spectra of M17 and M42. Data taken from the November 1974 and March-April 1975 field trips, and from Harper (1975). Error bars are one standard deviation, and the March-April 1975 data has been calibrated with the telescope offset. The curves plotted are diluted to fit the data.

two flights have not been used in the figure because of low signal to noise ratio on one night and lack of a wavelength calibration on the other, due to a slippage in the grating drive.

Efforts were made to fit the M17 spectrum with the sum of the emissions from grains at two different temperatures. The warmer grains were assumed to be at 150°K, this being the temperature suggested by preliminary results of 20μ to 40μ spectroscopy of M17 (Reed, 1975). This temperature is not very critical, since the slope does not vary much with temperature over the available bandpass of the spectrometer if the temperature is higher than 100°K. Various temperatures ranging from 25 to 40°K were tried for the cooler grains, these limits being suggested because grains warmer than 40°K would have their emission peaking below 70μ and would not fit the spectrum well, and grains cooler than 25°K would not emit enough to give the observed flux levels even if the source were optically thick over all the region covered by the beam of the spectrometer. Gray-body emissivities and emissivities proportional to λ^{-1} and λ^{-2} were tried for both the warm and cold components. None of these attempts gave a good fit to the observed spectrum.

The curve plotted on Figure 5-3 was fit to the results ignoring the points between 70μ and 80μ. It gave about as good a fit as could be obtained by the approach outlined above. The points between 70μ and 80μ were ignored because

instrumental effects are more important in that region of the spectrum, and because those points did not seem to fit the general trend of the spectrum. This will be discussed further in the following section.

Discussion of the M42 and M17 Spectra

Calibrations

The March-April 1975 data are by far the most interesting, simply because a wider bandpass is covered. However, the calibration for this data is somewhat problematical, and should perhaps be examined in greater detail.

As was mentioned earlier, overall calibration using moon data was not possible due to the nonlinearity of response, so the offset spectrum was used instead. The offset spectrum is obtained from the "sky" observations during observations of a source, so it is automatically at the same background as the observations of the source, since the sources we observe do not put out nearly enough flux to affect the background levels in the instrument. The offset signal is of local origin, probably coming from the inside of the telescope. The spectrometer sees almost the whole primary, and if the secondary chops slightly off-center some emission from the telescope barrel can reach the instrument. Hence it was assumed that the offset signal would have a color temperature corresponding to that of the inside of the telescope. This temperature is not well known, but should be close to the

temperature of the atmosphere outside the aircraft, which is about 230°K at observing altitudes. Therefore, this temperature was chosen for making the calibration. Errors in the temperature are not very critical, as blackbodies in this temperature range are almost in the Rayleigh-Jeans limit over the available bandpass of the spectrometer, and the slope varies slowly with temperature.

It is by no means obvious that the offset signal should have a blackbody spectrum. However, there are a number of facts which indicate that this may be the case. These are:

1. The inside of the telescope is coated with 3M Black Velvet paint, which absorbs (and hence emits) well even in the far infrared.
2. The spectrum of M42 after calibration with the offset agrees reasonably well with earlier M42 data (calibrated with the moon) between 75μ and 115μ.
3. Lunar calibrations are possible for the long wavelength data, after correction for nonlinearities, and these agree well with the offset calibrations.
4. The Venus data shown in Figure 5-4 fits a 245°K blackbody quite well, and has been calibrated using the offset. This is in agreement with observations of Venus by Chase et al. (1974) and atmospheric calculations (Ward, 1975) for Venus using a model from Marcov (1972) and assuming H_2O and CO_2 to be the most important sources of opacity in the far infrared.

The local origin of the offset emission causes one problem. Part of the purpose of a calibration source is to remove the effects of atmospheric transmission features, and the source emission passes through more water vapor than the offset emission does. However, many of the water vapor features are saturated even in the offset spectrum, so the difference is not as large as one might expect. Furthermore, the coarse resolution spectra are not very sensitive to water vapor features, simply because the spacing between water features is typically much less than the bandpass, and the water features tend to average out.

The offset signal turns out to be very stable from flight to flight, both in spectrum and in strength. This is reassuring, since it suggests that the spectrometer and telescope performance are the same from night to night.

This repeatability of performance is important when confronting the second major problem of the new two detector system, which is the lack of overlap between the two detectors. This was also discussed in Chapter II.

As can be seen from the Orion data, and from Venus data plotted in Figure 5-4, the long and short wavelength data mesh very well. This becomes important when the M17 data are considered, for there the break in the spectrum occurs in the 65μ to 70μ region, precisely where the overlap between detectors occurs. Only the fact that the Venus and M42 results mesh so well allows us to say with any confidence that

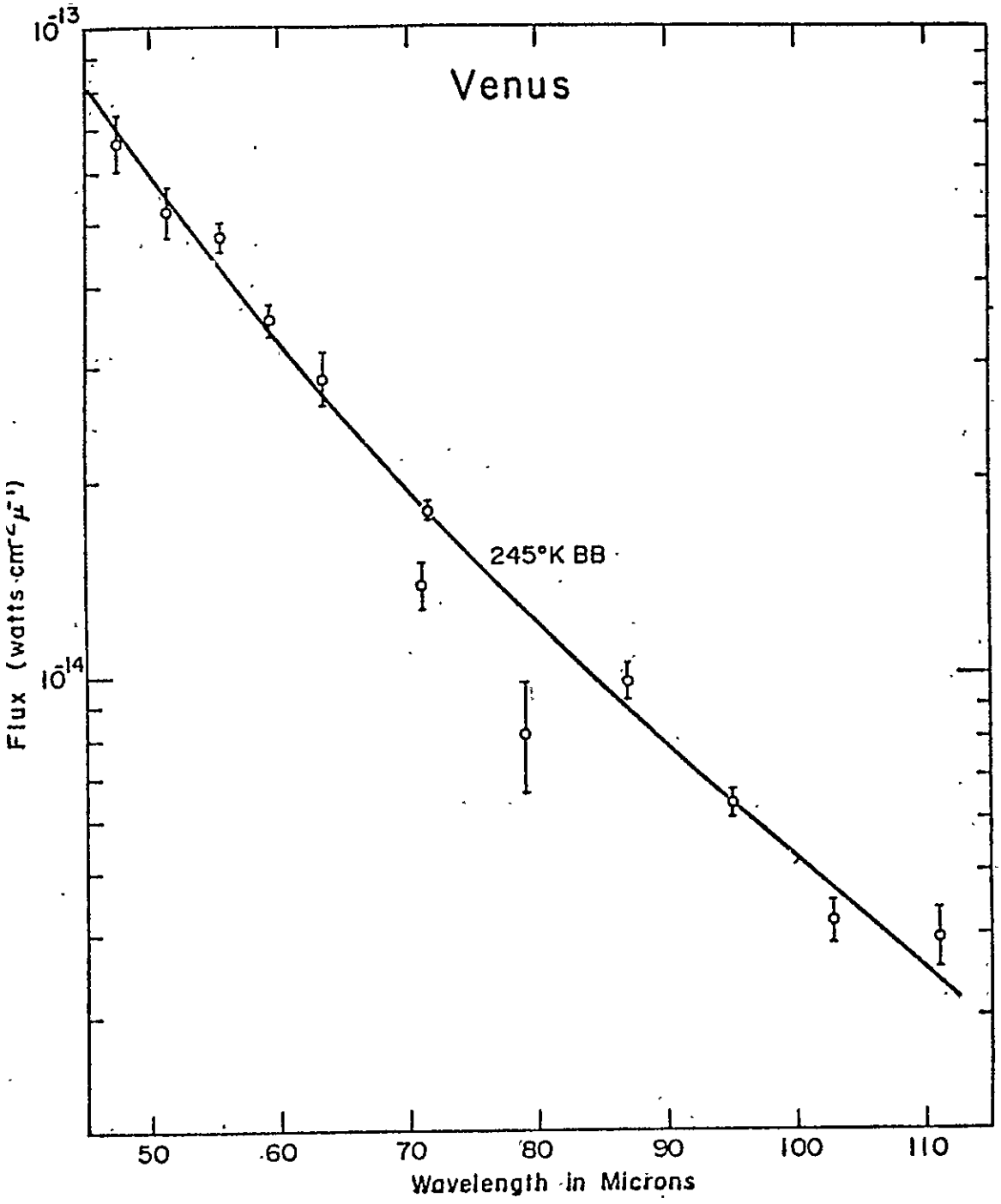

Figure 5-4. Spectrum of Venus from March-April 1975 field trip. Error bars are one standard deviation, and the telescope offset has been used for the calibration. The absolute flux scale assumes Venus to be a blackbody emitter at a temperature of 245°K.

the feature in M17 is real. Fortunately, it appears in data from three flights on M17, which adds to its credibility.

Dust Models

It is now fairly well accepted that the infrared emission from H II regions is thermal emission from dust grains. However, models for infrared emission from H II regions are still quite vague, which is not surprising considering that the composition of the interstellar grains is still largely unknown The probable dominant constituents are silicates, frozen water, graphite, iron, iron in compounds with sulphur, oxygen and silicates, and various simple and complex organic compounds (Harper et al., 1975). However, silicates and ice are the only constituents so far identified in infrared observations (Gillet and Forrest, 1973; Merrill and Soifer, 1974; Grasdalen, 1974).

In the following two subsections, the results from our observations will be compared to some of the models which have been suggested for M42 and M17.

M42

The M42 spectrum is very smooth, in agreement with the results published by other investigators (Erickson et al., 1973; Bandshaft et al., 1975) at lower signal to noise ratio and comparable resolution. The best fit temperature of 105°K agrees well with the temperature of 100°K derived by Houck et al., (1974) from spectral observations of M42 between

20μ and 40μ. Results of photometry at 400μ (Soifer and Hudson, 1974; Harper, 1973) are also consistent with the source emitting as a 100°K gray body. However, comparison of the results of Soifer and Hudson with the fluxes detected by Harvey et al. (1974) at 1 mm indicates that beyond 400μ the grain emissivity has a λ^{-2} dependence.

Houck et al. (1974) describe two isothermal models which would yield such a spectrum. One model envisions the source as containing grains whose emissivity varies as λ^{-2}. These grains are in dense clumps which are optically thick out to 400μ. A number of these clumps covering roughly 10% of the 2 arc minute area surrounding the Kleinmann-Low nebula would give the observed spectrum and flux. The second model employs grains with impurities and structural dislocations which yield enhanced emissivity at long wavelengths. Such grains have been suggested by Hoyle and Wickramasinghe (1969). If such grains had constant emissivity out to 400μ, a 2 arc minute cloud with optical depth 0.1 would produce the observed spectrum and flux.

The real situation in the source is almost certainly more complicated than these models. Evidence for more complexity comes from the maps of M42 with 1 arc minute resolution at 20μ, 50μ and 100μ which have been made by Werner et al. (1975). Their maps cover roughly the same area surveyed by our beam, and show variations in the 50μ to 100μ color temperature over this region, with emission at 100μ being more extended.

Thus the spectrum we observe is really a composite of the spectra of a number of smaller regions with different temperatures and possibly different dependence of emissivity on wavelength.

From our results, it would appear that the distribution of temperature and composition must be fairly smooth across the source, simply because the overall spectrum is so smooth. However, spectral observations with a smaller beam are necessary in order to get more detailed information on the source structure.

M17

The spectrum of M17 has a bump at about 70μ and a general far infrared excess, in contrast to the very smooth spectrum of M42. A simple approach to explaining such a spectrum is by means of a distribution of grains of two different temperatures. The hot grains are responsible for the short wavelength emission while the cooler grains emit at longer wavelengths. Such a distribution of grain temepratures has been suggested by Lemke and Low (1972) and Wright (1973) in order to explain the very broad spectrum of M17, which is very bright at 10μ and 20μ as well as in the far infrared.

In Wright's model, the near infrared radiation comes from grains inside the ionized region of the nebula, while the far infrared emission comes from dust in neutral regions outside the ionized volume. Inside the H II region, dust has been depleted, so that opacity is low for photons of wavelength

longer than 912A. These photons escape to the outside, where they heat the dust in the neutral region, which supplies the far infrared emission. The dust inside the nebula is heated by nebular Lyman α photons, and produces the emission in the "middle infrared" at 10μ and 20μ. Wright's model ignores the effects of variations in size and composition of the grains, and assumes that the emissivity is proportional to λ^{-1}. One result of his model is that the 100μ emission should come from a shell surrounding the H II region.

Lemke and Low (1972) have suggested that two types of grains exist within the ionized portion of the nebula. One type of grain has good emissivity in the far infrared. This type of grain absorbs ultraviolet and optical photons well, but stays cold because it can get rid of the energy in the form of far infrared emission. The second type of grain has poorer infrared emissivity, and cannot cool itself as readily. Hence it heats up and supplies the near infrared emission. The two types of grains are both inside the H II region, and in this model the bulk of the far infrared and middle infrared emission comes from the ionized portion of the nebula.

As seen in the previous section, a simple two temperature model does not fit the observed spectrum well. In particular, it is difficult to produce the bump between 63μ and 87μ with such a model, which tends to yield a much smoother spectrum. Part of this feature may be due to instrumental effects, as the instrumental response has a steep slope in

this region of the spectrum. It is hard to completely explain away the feature with instrumental effects, but more observations with better system response over this spectral region are necessary to really confirm it.

Even when ignoring the data between 63μ and 87μ, it is difficult to fit the remaining points with the simple approach described in the last section. However, the large far infrared excess is probably real, since it showed up in data from three flights, while no long wavelength excess appeared for either Venus or M42. A two component model in which the wavelength dependence of the emissivity varies with wavelength might fit the observed spectrum better.

The most striking feature of the two component explanation for the spectrum of M17 is the very cold temperature required for the component responsible for the far infrared emission. Even if it is assumed that the grains radiate as gray bodies throughout the far infrared, the temperature must be less than 40°K to give the spectrum observed. Putting in emissivity effects makes the grains have to be still colder in order to match the spectrum, since the peak of their emission shifts to shorter wavelengths than in the gray body case.

The temperature of these grains can be used to give some idea of their optical properties. If the nebula is optically thin in the far infrared, the optical depth at wavelength λ is given by

$$\tau_\lambda = \frac{F_\lambda}{B_\lambda(T)\ \Omega}$$

where Ω is the solid angle of the region observed, F_λ is the flux density detected at wavelength λ, and $B_\lambda(T)$ is the intensity per steradian emitted by a blackbody at temperature T.

A rough value for the optical depth can be obtained by assuming that the emissivity of the grains has a wavelength dependence proportional to λ^{-1}. The temperature for the best fit is then about 30°K, and if we take $\lambda = 95\mu$, and use the measured beam size of the instrument to get Ω, we obtain an optical depth of 0.18.

If we now define Q_λ to be the ratio of the absorption cross-section at wavelength λ to the geometrical cross-section, then the mass of grains in the region we observe is

$$M_d = \frac{\tau_\lambda}{Q_\lambda} \left(\frac{A}{4\pi a^2}\right) \rho \frac{4}{3} \pi a^3$$

where a is the average grain radius (assuming spherical grains), A is the area covered by the beam at the source, and ρ is the average grain density. Using the distance of 2.2 kpc for M17 from Schraml and Mezger (1969), and assuming $\rho = 2.3$ gm cm^{-3} and $a = 0.05\mu$ as does Panagia (1974), we get from the calculation of the optical depth that the dust mass in solar masses m_o is

$$M_d = \frac{0.027\ m_o}{Q_{95\mu}}$$

If we now assume that the far infrared emission comes from the ionized portion of the nebula, in agreement with the suggestion of Lemke and Low, we can use the value of 334 solar masses derived by Schraml and Mezger (1969) for the ionized mass of the nebula, and get for the dust to gas ratio

$$\frac{M_d}{M_g} = \frac{8 \times 10^{-5}}{Q_{95\mu}}$$

This ignores the mass of the dust that is responsible for the middle infrared emission, but the optical depth required for this dust to produce the emission seen at 55μ is only about 0.001, so the mass involved is much smaller.

The interstellar average value for the dust to gas ratio is roughly 0.01 (Jenkins and Savage, 1972), and this is also the average value derived by Panagia (1974) using his model calculations and the infrared data of Emerson, Jennings and Moorwood (1973). If we assume this value, then

$$Q_{95\mu} = 0.008$$

This value is quite high, much higher than the predictions for silicate grains, with or without ice mantles (Knacke and Thompson, 1973; Leung, 1975). However, if a λ^{-1} emissivity law is assumed, there is reasonable agreement with the value of 0.01 at 50μ suggested by Panagia.

If a large proportion of the emission is coming from neutral clouds outside the H II region, the gas to dust ratio limitations are less stringent, since the molecular clouds surrounding M17 are considerably more massive than the H II region (Lada and Chaisson, 1975; Lada et al., 1974). However, from the map of Harper et al. (1975), it seems that the 100μ emission is coming from the ionized region instead of the molecular clouds seen by Lada et al. There are some cold extensions which radiate at 100μ, but the majority of the emission is in the same direction as the thermal radio emission at 1.95 cm seen by Schraml and Mezger. The map is at fairly coarse spatial resolution (2.2 arc minutes), however, and a shell structure may still show up in maps made with a smaller beam.

Future Observations

The instrumental sensitivity at coarse resolution is now good enough to make possible detection of a wide variety of objects, and some of these sources are given in Table 5-1. In the future we hope to make observations of as many of these sources as possible.

Table 5-1. Some Observable H II Regions.

Source	Wavelength	Flux (Harper, 1974) (watts cm^{-2} μ^{-1})	Signal/Noise in one second
M42	91μ	1.1×10^{-14}	~25
M17	93μ	4.1×10^{-15}	~10
NGC 2024	100μ	1.7×10^{-15}	~ 4
SGR A	91μ	2.6×10^{-15}	~ 7
SGR B	100μ	2.4×10^{-15}	~ 6
W3 (G133.7+1.2)	94μ	2.2×10^{-15}	~ 5

BIBLIOGRAPHY

Armstrong, K.R., Harper, D.A., and Low, F.J., Ap.J. (Letters), 177, L21, 1972.

Armstrong, K.R., and Low, F.J., Applied Optics, 12, 2007, 1973.

Aller, L.H., and Liller, W., in Nebulae and Interstellar Matter, ed. B.N. Middlehurst and L.H. Aller (Chicago: University of Chicago Press), 1968.

Bergeron, J., private communication, 1975.

Brandshaft, D., McLaren, R.A., and Werner, M.W., Ap.J. (Letters), 199, 115, 1975.

Chase, S.C., Miner, E.D., Morrison, D., Munch, G., and Neugebauer, G., Science, 183, 1291, 1974.

Emerson, J.P., Jennings, R.E., and Moorwood, A.F.M., Ap.J., 184, 401, 1973.

Erickson, E.F., Swift, C.D., Witteborn, F.C., Mord, A.J., Augason, G.C., Caroff, L.J., Kunz, L.W., and Giver, L.P., Ap.J., 183, 535, 1973.

Erickson, E.F., Goorvitch, D., Dix, M.G., and Hitchman, M.J., Lear Jet Telescope System, NASA TM X-62,389, 1974.

Fazio, G.G., Kleinmann, D.E., Noyes, R.W., Wright, E.L., Zeilik, M., and Low, F.J., Ap.J. (Letters), 192, L23, 1974.

Forrest, W.J., private communication, 1975.

Gillett, F.C., and Forrest, W.J., Ap.J., 179, 483, 1973.

Grasdalen, G.L., Ap.J., 193, 373, 1974.

Harper, D.A. and Low, F.J., Ap.J. (Letters), 165, L9, 1971.

Harper, D.A., Low, F.J., Rieke, G.H. and Armstrong, K.R., Ap.J. (Letters), 177, L21, 1972.

Harper, D.A., Ap.J., 192, 557, 1974.

Harper, D.A., Low, F.J., Rieke, G.H., and Thronson, H.A. Yerkes Observatory Preprint No. 154, 1975.

Harvey, P.M., Gatley, I., Werner, M.W., Elias, J.H., Evans, N.J., Zuckerman, B., Morris, G., Sato, T. and Litvak, M.M., Ap.J. (Letters), 189, L87, 1974.

Hoffman, W.F., Frederick, C.L. and Emery, R.J., Ap.J. (Letters), 170, L89, 1971.

Houck, J.R., Schaack, D.F. and Reed, R.A., Ap.J. (Letters), 193, L139, 1974.

Hoyle, F. and Wickramasinghe, N.C., Nature, 223, 459, 1969.

Jenkins, E.B. and Savage, B.D., IAU Symposium No. 52, 1972.

Knacke, R.F. and Thompson, R.K., Pub. A.S.P., 85, 341. 1973.

Lada, C., Dickinson, D.F. and Penfield, H., Ap.J. (Letters), 189, L35, 1974.

Lada, C., and Chaisson, E.J., Ap.J., 195, 367, 1975.

Lemke, D. and Low, F.J., Ap.J. (Letters), 177, L53, 1972.

Leung, C.M., Ap.J., 199, 340, 1975.

Low, F.J., Aumann, H.H. and Gillespie, C.M., Astronautics and Aeronautics, 7, 26, 1970.

Linsky, J.L., Ap.J. Suppl., 25, 163, 1973.

Marov, M. Ya., Icarus, 16, 415, 1972.

McClatchey, R.A., Benedict, W.S., Clough, S.A., Burch, D.E., Calfee, R.F., Fox, K., Rothman, L.S., and Garing, J.S., AFCRL Technical Report 73-0096, 1973.

Merrill, K.M. and Soifer, B.T., Ap.J. (Letters), 189, L27, 1974.

Moore, W.J. and Shenker, H., Infrared Physics, 5, 99, 1965.

Osterbrock, D.E. and Flather, E., Ap.J., 129, 26, 1959.

Panagia, N., Ap.J., 192, 221, 1974.

Petrosian, V., Ap.J., 159, 833, 1970.

Pipher, J.L., Ph.D. Dissertation, C.R.S.R. Report No. 461, 1971.

Reed, R.A., private communication, 1975.

Schaack, D.F., private communication, 1975.

Schraml, J. and Mezger, P.G., Ap.J., 156, 269, 1969.

Simpson, J.P., Pub. A.S.P., 85, 479, 1973.

Simpson, J.P., Astron. and Astrophys., 39, 43, 1975.

Soifer, B.T., Pipher, J.L. and Houck, J.R., Ap.J., 177, 315, 1972.

Soifer, B.T., and Hudson, H.S., Ap.J. (Letters), 191, L83, 1974.

Ward, D.B., unpublished, 1975.

Werner, M.W., Gatley, I., Harper, D.A., Becklin, E.E., Loewenstein, R.F., Telesco, C.M. and Thronson, H.A., in press, 1975.

Wright, E.L., Ap.J., 185, 569, 1973.

Zuckerman, B., Ap.J., 183, 863, 1973.